OPALS.JL: A COMPREHENSIVE, COMPOSABLE FRAMEWORK FOR DATA ASSIMILATION IN JULIA

NICHOLAS MUELLER†

arXiv:2608.24265v1 [cs.MS] 25 Aug 2026

ABSTRACT. Data assimilation (DA) and inverse modelling are indispensable tools for combining physics-based models with observations, yet the software that implements them is often fragmented: sequential (Kalman and particle) filters and variational (3D/4D-Var) estimators are typically developed as separate codebases, each tied to a specific class of forward model – for example, simple time-marching schemes for ordinary differential equations (ODEs), or full finite element (FE) discretisations of partial differential equations (PDEs). In this work, we present OPALS.JL, a Julia package that overcomes this fragmentation by providing a unified environment for a wide range of DA methods and forward model backends, all accessible behind a single high-level interface. Starting from a handful of basic methods, complex inference tools can be built by composing them with advanced capabilities, such as covariance localisation/inflation, online noise covariance estimation, bias-aware correction, and kriging-based calibration of reduced-order surrogates. The package integrates natively with the SciML ecosystem for ODE-governed systems, and with Gridap/GridapROMs for both full-order and reduced-order discretisations of PDEs. Notably, the API is designed to allow a reduced-order surrogate to replace a full-order solver with no change to the code, even at the driver level. We demonstrate the library on a Lorenz-63 benchmark, on a Van der Pol oscillator problem with biased observations, on a turbulent Navier-Stokes flow past a square cavity, where the unknown Reynolds number is inferred from sparse velocity and pressure measurements, and finally on a heat equation using a reduced-order surrogate instead of a more standard full-order model.

Program summary

Program Title: Opals.jl: Open source Probabilistic & Assimilation Library for Simulations in Julia
Program Version: 0.1.0
Developer's repository link: https://github.com/nichomueller/Opals.jl
Licensing provisions: MIT license
Programming language: Julia
Nature of problem: Estimating the hidden state and, where relevant, the uncertain parameters of any dynamical system from observational data that are partial, corrupted by noise, and potentially biased. Such problems are generally ill-posed and computationally demanding, since they usually rely on a forecast-and-analyse paradigm, with the forecasting step being potentially expensive. Practitioners typically lack a single and mature software environment across heterogeneous forward model backends – lightweight ODEs and full-order PDE discretisations alike – without extensive re-implementation.
Solution method: Opals.jl exposes a single, type-driven interface to both Bayesian sequential filters (Kalman, extended Kalman, unscented, ensemble Kalman variants, and particle filters) and variational methods (3D-Var, 4D-Var), all sharing the same execution, composition, and diagnostic pipeline. Advanced capabilities – covariance localisation and inflation, surrogate model calibration, and bias-aware correction – are added incrementally as composable wrappers around a common filter interface. The library integrates natively with the SciML ecosystem for ODE-governed models and with Gridap/GridapROMs for both full-order and reduced-order PDE models, thus enabling a wide range of applications to be tackled with multiple methodologies all sharing the same pipeline.

1. INTRODUCTION

The solution of inverse problems is a fundamental task across the sciences and engineering, including meteorology [1, 2], oceanography [3, 4], hydrology [5], and geophysics [6]. Inverse problems seek to estimate unknown parameters and/or unobserved states of a system from data measurements that are partial and corrupted by noise. Because such problems are typically ill-posed [7], their robust and efficient solution is essential for reliable forecasting.

Data assimilation (DA) is a particularly well-developed instance of this general problem, in which a forward model (often high-dimensional and nonlinear), describing some physical process, is combined with observations to estimate an evolving hidden state and, in many cases, uncertain model parameters. Two methodological families have matured largely in parallel: sequential Bayesian filters – among which Kalman filters (KFs) [8] and particle filters [9] are especially popular – and variational methods, such as the 3D- and 4D-Var [10, 11]. Despite the two families being conceptually overlapping, the corresponding software has remained comparatively fragmented: the two approaches are rarely available together in open-source packages and are typically decoupled from the forward model backend, so that switching from a hand-written prototype to a dynamical system based on the finite element (FE) discretisation of a partial differential equation (PDE) requires substantial re-engineering. In practice, this forces users to reimplement even straightforward routines such as observation handling, ensemble bookkeeping, and diagnostics for every new combination of method and model, slowing methodological comparison and greatly reducing productivity.

†FACULTY OF CIVIL ENGINEERING AND GEOSCIENCES, TU DELFT, DELFT, THE NETHERLANDS
Date: August 26, 2026.

The Julia ecosystem already provides mature, well-established packages that individually address parts of this landscape, though none spans it entirely. EnsembleKalmanProcesses.jl [12] implements ensemble Kalman filter (EnKF)- and unscented Kalman filter (UKF)-based inversion for calibrating black-box models, but it lacks several hallmarks of sequential state-estimation theory and features no backends for ordinary differential equation (ODE)/PDE-based modelling. LowLevelParticleFilters.jl [13] offers an established implementation of the extended Kalman filter (EKF), UKF, and particle filters for state estimation, but does not extend to variational estimation and suffers from a similarly restricted scope of applications. General-purpose probabilistic-programming packages such as Turing.jl [14] and Gen.jl [15] support Bayesian inference over essentially arbitrary generative models, but are more focused on regression and Markov chain Monte Carlo (MCMC) sampling strategies than on DA-specific filtering, and have not been applied to large-scale PDE-constrained state estimation. Within the SciML ecosystem itself, DiffEqParamEstim.jl and SciMLSensitivity.jl [16] provide optimisation- and adjoint-based parameter fitting for ODEs, addressing deterministic parameter estimation but not Bayesian inference, advanced bias-correction capabilities, or PDE modelling. On the other hand, uncertainty quantification (UQ)-oriented packages such as UncertaintyQuantification.jl [17] and GlobalSensitivity.jl [18] provide Monte Carlo (MC), polynomial-chaos, and sensitivity-analysis methods for propagating uncertainty through a model, but are not organised around a DA loop. Additionally, none of the above address the need for combining DA with reduced order models (ROMs), whose use is paramount for large-scale PDE-based applications.

Against this background, Opals addresses the lack of a unified and extensible framework for DA and inverse modelling by bringing together modern algorithms for sequential filtering and variational estimation across a broad range of forward models. Several of these capabilities are currently absent from existing Julia frameworks and are rarely available together within a single computational ecosystem. Leveraging Julia's multiple dispatch and just-in-time (JIT) compilation, Opals combines efficiency and flexibility while exposing these methods through a common interface applicable to forward models ranging from arbitrary ODE systems to FE-discretised PDEs and their ROM counterparts.

A second contribution is a compositional design that avoids embedding advanced capabilities into monolithic algorithm implementations. Instead, Opals expresses extensions as wrappers around a shared filter interface: covariance localisation [19], multiplicative and innovation-adaptive covariance inflation [20], adaptive noise covariance estimation [21], kriging-based calibration of reduced-order surrogates [22], and bias correction through reservoir computing (RC)-based architectures [23] can each be incorporated incrementally around an existing filter. New filters can be added either by combining existing wrappers or by implementing the interface directly, without changes to the existing codebase.

A third contribution is interoperability with established scientific-computing ecosystems. For ODE-based dynamics, a thin layer allows us to use arbitrary SciML integrators directly as forward models. For PDE-based dynamics, Opals interfaces with Gridap [24] and GridapROMs [25], enabling the solutions – either full-order or reduced-order – to be assimilated by any filtering method in the library without modification of the assimilation workflow beyond replacing the transition model. Consequently, a cheap surrogate can replace the corresponding full-order model purely as a computational acceleration. This integration connects DA methodology with modern discretised physics models, overcoming software boundaries that traditionally limit the transfer of methods between algorithm development and simulation frameworks operating at different fidelities.

The paper is organised as follows. Section 2 formalises the estimation problem and introduces the methodologies implemented in Opals. Section 3 describes the package architecture, composable wrapper mechanism, SciML and Gridap/GridapROMs interoperability layers, and a fully commented usage example. Section 4 demonstrates the capabilities of the framework on four challenging benchmarks spanning chaotic ODE and PDE dynamics. First, a Lorenz-63 system is addressed with multiple different Bayesian and variational methods. Second, a Van der Pol oscillator problem with biased observations is solved with a RC-corrected, bias-aware ensemble filter. Third, a turbulent two-dimensional Navier-Stokes flow around a square cavity showcases joint state-parameter estimation through the identification of the unknown Reynolds number via DA. Lastly, a parametrised heat equation demonstrates the replacement of a full-order PDE solver by a reduced-order surrogate, with kriging-based calibration compensating for the associated loss of accuracy. Code snippets for the usage example in Section 3 and the numerical experiments are reported throughout the body of the paper. Finally, Section 5 concludes the paper with a summary of the content and future directions of research.

2. Problem description and methods

This section lays the mathematical foundations of the problems addressed by Opals. Subsection 2.1 formalises the class of joint state-parameter inverse models targeted by the package. Subsection 2.2 and 2.3 derive the classical KF and its ensemble variants as the two basic instances of this framework, while Subsection 2.4 discusses the auxiliary inflation, localisation, and adaptivity techniques that increase the stability and accuracy of the EnKFs across different applications. Subsections 2.5 and 2.6 extend the filter to account for two distinct sources of structural model error – systematic observation bias and the error introduced by a reduced-order surrogate – through a RC-based and a kriging-calibrated bias model, respectively. Subsection 2.7 provides a brief overview of the remaining Bayesian methodologies implemented in the package (the UKF and particle filters), while Subsection 2.8 closes the section by discussing variational (3D-/4D-Var) methods.

2.1. **The model.** By and large, we are interested in the following class of inverse problems: given a set of observations of a system governed by a parameterised system of equations, we aim to jointly recover an unknown state variable and a

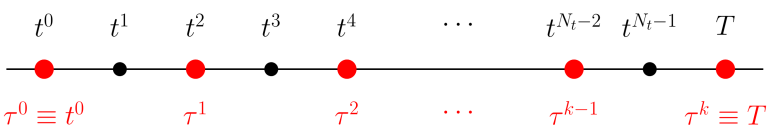

FIGURE 1. Integration stencil for the transition model (in black) and observation stencil (in red).

parameter vector that best explain the observations. This problem is described by a constrained optimisation problem

$$\begin{aligned} &\arg\min_{(\boldsymbol{\mu},\boldsymbol{u})} \ \mathcal{L}(\boldsymbol{u}(\boldsymbol{\mu});\boldsymbol{\mu}) \doteq \frac{1}{2}\left\|\boldsymbol{\mathcal{G}}(\boldsymbol{u}(\boldsymbol{\mu})) - \boldsymbol{u}_{\text{obs}}\right\|^2_{\boldsymbol{\Sigma}^{-1}}, \\ &\text{subject to} \quad \frac{d\boldsymbol{u}(\boldsymbol{\mu})}{dt} + \boldsymbol{\mathcal{A}}(\boldsymbol{u}(\boldsymbol{\mu});\boldsymbol{\mu}) = \boldsymbol{0}, \end{aligned} \tag{1}$$

where $\boldsymbol{u}(\boldsymbol{\mu}) \in \mathbb{R}^{N_u}$ is the state variable, $\boldsymbol{\mu} \in \mathbb{R}^{N_\mu}$ is the parameter vector, $\boldsymbol{\mathcal{G}} : \mathbb{R}^{N_u} \to \mathbb{R}^{N_{\text{obs}}}$ is the *observation* operator, $\boldsymbol{u}_{\text{obs}} \in \mathbb{R}^{N_{\text{obs}}}$ are the observations, and $\boldsymbol{\Sigma} \in \mathbb{R}^{N_{\text{obs}} \times N_{\text{obs}}}$ is a symmetric, positive-definite weighting matrix specified shortly. The operator $\boldsymbol{\mathcal{A}}$ describes the dynamics of the system – which may be governed, for example, by a set of ODEs or PDEs – and is commonly referred to as the *forward* or *transition* model. The operator $\boldsymbol{\mathcal{G}}$ is usually linear, that is

$$\boldsymbol{\mathcal{G}}(\boldsymbol{u}) = \boldsymbol{G}\boldsymbol{u} \ \ (+\boldsymbol{b}), \qquad \boldsymbol{G} \in \mathbb{R}^{N_{\text{obs}} \times N_u}, \boldsymbol{b} \in \mathbb{R}^{N_{\text{obs}}}, \tag{2}$$

where $\boldsymbol{b}$ is an optional bias term, which may be included to account for systematic errors in the observations. There are many examples of bias-aware implementations in the literature, including *in-situ* bias estimation and correction [26, 27], and hybrid bias-aware DA [28, 29]. In very simple terms, the former estimates the bias as part of the assimilation framework, whereas the latter decouples these two tasks and is generally credited with greater flexibility and complexity in the bias model [23]. The treatment of bias is central to the present work, and we will return to it in Subsections 2.5-2.6.

In practice, however, neither $\boldsymbol{\mathcal{A}}$ nor $\boldsymbol{\mathcal{G}}$ are known exactly. A standard way to represent the uncertainty associated with these operators is by introducing additive Gaussian noise, that is

$$\boldsymbol{\mathcal{A}}_{\boldsymbol{\theta}}(\cdot) \doteq \boldsymbol{\mathcal{A}}(\cdot) + \boldsymbol{\theta}, \qquad \boldsymbol{\mathcal{G}}_{\boldsymbol{\sigma}}(\cdot) \doteq \boldsymbol{\mathcal{G}}(\cdot) + \boldsymbol{\sigma},$$

where $\boldsymbol{\theta} \sim \mathcal{N}(\boldsymbol{0}, \boldsymbol{\Theta})$ and $\boldsymbol{\sigma} \sim \mathcal{N}(\boldsymbol{0}, \boldsymbol{\Sigma})$ are independent, zero-mean Gaussian random variables. Note that the covariance matrix $\boldsymbol{\Sigma}$ for the observation noise corresponds to the weight employed in Eq. (1) for the observation misfit. Following the standard DA and UQ literature – see, e.g., the seminal work of Kalman [8] – the true pair $(\boldsymbol{\mu}^\star, \boldsymbol{u}^\star)$, i.e., the one actually realising the observations through the unknown true system, is assumed to satisfy not Eq. (1) but rather the stochastic problem

$$\begin{aligned} \frac{d\boldsymbol{u}^\star(\boldsymbol{\mu}^\star)}{dt} + \boldsymbol{\mathcal{A}}_{\boldsymbol{\theta}^\star}(\boldsymbol{u}^\star(\boldsymbol{\mu}^\star);\boldsymbol{\mu}^\star) &= \boldsymbol{0}, \\ \boldsymbol{u}_{\text{obs}} &= \boldsymbol{\mathcal{G}}_{\boldsymbol{\sigma}^\star}(\boldsymbol{u}^\star(\boldsymbol{\mu}^\star)), \end{aligned} \tag{3}$$

with $\boldsymbol{\theta}^\star \sim \mathcal{N}(\boldsymbol{0}, \boldsymbol{\Theta})$ and $\boldsymbol{\sigma}^\star \sim \mathcal{N}(\boldsymbol{0}, \boldsymbol{\Sigma})$. That is, the transition and observation operators governing the true dynamics are themselves stochastic, so that recovering $(\boldsymbol{\mu}^\star, \boldsymbol{u}^\star)$ from $\boldsymbol{u}_{\text{obs}}$ is fundamentally a Bayesian inference problem rather than a deterministic optimisation problem. Therefore, the goal is to find a distribution (usually a two-moment law, most commonly a Gaussian) over the state and parameter vectors that best represents our uncertainty about their true values. In the following subsections, we describe some of the methodologies implemented in Opals to solve this problem, including the classical KF, its variants, and variational strategies.

2.2. **Kalman filter.** The classical KF is a sequential algorithm that provides an optimal solution to (3) under the assumptions of linearity of both transition and observation operators, and Gaussianity (more on this in the next paragraph). It consists of two main steps: the *forecast* step, where the current state estimate is propagated forward in time using the model dynamics, and the *analysis* step, where the forecast is corrected using new observations. Rather than estimating the state and parameters separately, we consider the augmented variable $\boldsymbol{x} \doteq (\boldsymbol{\mu}, \boldsymbol{u})^T \in \mathbb{R}^{N_x}$, where $N_x \doteq N_\mu + N_u$, and estimate both jointly with every filter discussed in this and the following subsections. For the time being, we consider an unbiased linear observation model ($\boldsymbol{b} \equiv \boldsymbol{0}$). Discretising Eq. (3) in time over a partition $t^0 < t^1 < \cdots < t^{N_t} \equiv T$ gives

$$\boldsymbol{x}^k = \boldsymbol{\mathcal{F}}_{\boldsymbol{\theta}}(\boldsymbol{x}^{k-1}), \qquad \forall k = 1, \ldots, N_t \tag{4}$$

$$\boldsymbol{u}^k_{\text{obs}} = \boldsymbol{H}\boldsymbol{x}^k + \boldsymbol{\sigma}^k, \qquad \forall k = 1, \ldots, N_t \tag{5}$$

where $\boldsymbol{\mathcal{F}}_{\boldsymbol{\theta}}$ is a block-diagonal operator obtained by concatenating (i) a $N_\mu \times N_\mu$ identity matrix – acting on the parameter block – and (ii) the integral of $\boldsymbol{\mathcal{A}}_{\boldsymbol{\theta}}$ over (t^{k-1}, t^k) – acting on the state variable. $\boldsymbol{H} \in \mathbb{R}^{N_{\text{obs}} \times N_x}$ denotes the observation matrix of Subsection 2.1, implicitly augmented with a zero block on the parameter component since observations depend on the state alone. Note that the expressions of both $\boldsymbol{\mathcal{F}}_{\boldsymbol{\theta}}$ and $\boldsymbol{H}$ may depend on the time index k, though we will henceforth assume they do not. Also, as shown in Fig. 1, the observations need not occur at every integration step. On the contrary, it is quite common for observations to be sparse in time ($k < N_t$) and in space ($N_{\text{obs}} < N_u$, and potentially $N_{\text{obs}} \ll N_u$).

Sparse observations create challenges, as they increase the complexity of accurately constraining and estimating the evolution of the system [30]. Although we will consider missing observations in the numerical experiments in Section 4, for simplicity, we will assume for the present that observations are available at each integration step.

Consider a single cycle of the recursion, from the previous analysis $\boldsymbol{x}_a^{k-1}$ to the next one $\boldsymbol{x}_a^k$; to keep the notation light, we drop the time index for the remainder of this derivation. The forecast step propagates the previous analysis through $\boldsymbol{\mathcal{F}}_{\boldsymbol{\theta}}$, producing a forecast $\boldsymbol{x}_f$ and an associated covariance $\boldsymbol{P}_f$, which is computed as

$$\boldsymbol{P}_f = \boldsymbol{F}\boldsymbol{P}_a\boldsymbol{F}^T + \boldsymbol{\Pi},$$

where $\boldsymbol{F} \in \mathbb{R}^{N_x \times N_x}$ is the Jacobian of $\boldsymbol{\mathcal{F}}_{\boldsymbol{\theta}}$ at the previous analysis, $\boldsymbol{\Pi} \in \mathbb{R}^{N_x \times N_x}$ is the covariance of the process noise (usually block-diagonal, with a zero block on the parameter component), and $\boldsymbol{P}_a$ is the previous analysis covariance. We refer to [8] for more details. We always assume that the forecast step produces a Gaussian prior[1] for $\boldsymbol{x}$, that is $\boldsymbol{x} \sim \mathcal{N}(\boldsymbol{x}_f, \boldsymbol{P}_f)$. The analysis step then uses the new observation $\boldsymbol{u}_{\text{obs}}$ to characterise the posterior $p(\boldsymbol{x} \mid \boldsymbol{u}_{\text{obs}}) \propto p(\boldsymbol{u}_{\text{obs}} \mid \boldsymbol{x})\, p(\boldsymbol{x})$ via Bayes' theorem. Both the prior and the observation likelihood implied by Eq. (4) are Gaussian,

$$p(\boldsymbol{x}) \propto \exp\left(-\frac{1}{2}\|\boldsymbol{x} - \boldsymbol{x}_f\|^2_{\boldsymbol{P}_f^{-1}}\right), \qquad p(\boldsymbol{u}_{\text{obs}} \mid \boldsymbol{x}) \propto \exp\left(-\frac{1}{2}\|\boldsymbol{u}_{\text{obs}} - \boldsymbol{H}\boldsymbol{x}\|^2_{\boldsymbol{\Sigma}^{-1}}\right),$$

with the latter being a consequence of the linearity of Eq. (5). The posterior is itself Gaussian by virtue of Bayes' theorem:

$$p(\boldsymbol{x} \mid \boldsymbol{u}_{\text{obs}}) \propto \exp(-\mathcal{L}_{\text{KF}}(\boldsymbol{x})), \qquad \mathcal{L}_{\text{KF}}(\boldsymbol{x}) \doteq \frac{1}{2}\|\boldsymbol{x} - \boldsymbol{x}_f\|^2_{\boldsymbol{P}_f^{-1}} + \frac{1}{2}\|\boldsymbol{u}_{\text{obs}} - \boldsymbol{H}\boldsymbol{x}\|^2_{\boldsymbol{\Sigma}^{-1}}.$$

The analysis step can be derived by seeking the minimiser of $\mathcal{L}_{\text{KF}}$. Imposing first-order optimality condition and performing some algebraic manipulations (among which the Woodbury identity [31]) gives

$$\boldsymbol{x}_a = \boldsymbol{x}_f + \boldsymbol{K}\left(\boldsymbol{u}_{\text{obs}} - \boldsymbol{H}\boldsymbol{x}_f\right), \qquad \boldsymbol{P}_a = (\boldsymbol{I} - \boldsymbol{K}\boldsymbol{H})\boldsymbol{P}_f, \qquad \boldsymbol{K} \doteq \boldsymbol{P}_f\boldsymbol{H}^T\left(\boldsymbol{H}\boldsymbol{P}_f\boldsymbol{H}^T + \boldsymbol{\Sigma}\right)^{-1}, \tag{6}$$

where $\boldsymbol{K} \in \mathbb{R}^{N_x \times N_{\text{obs}}}$ is the *Kalman gain*, an optimal weighting between the forecast and the (noisy) observation. Equations (4)–(6) define one cycle of the KF. Because $\boldsymbol{\mathcal{A}}_{\boldsymbol{\theta}}$, and hence $\boldsymbol{\mathcal{F}}_{\boldsymbol{\theta}}$, is generally nonlinear, this linearise-and-correct recursion is more precisely the EKF [32]; it reduces to the classical linear KF whenever $\boldsymbol{\mathcal{A}}_{\boldsymbol{\theta}}$ is itself linear, in which case $\boldsymbol{F}$ no longer depends on the point at which it is evaluated.

The recursion is sequential by construction, updating the joint state-parameter estimate as each new observation arrives, which makes it naturally suited to DA pipelines. It is, however, subject to several limitations that motivate the variants discussed in the remainder of this section:

- Its optimality (in the minimum-variance sense) only holds under the linear and Gaussian assumptions, which are often violated in practice.
- The process- and observation-noise covariances $\boldsymbol{\Pi}^k$ and $\boldsymbol{\Sigma}^k$ are ordinarily assumed to be constant in time, though they may instead be estimated sequentially when this assumption is untenable [33].
- Propagating the full covariance $\boldsymbol{P}_a^k$ costs $\mathcal{O}(N_x^3)$ per step, which becomes prohibitive for large-scale problems and is the main motivation for the ensemble-based approximations introduced next.
- The innovation, $(\boldsymbol{u}_{\text{obs}} - \boldsymbol{H}\boldsymbol{x})$, represents the difference between the observations and their corresponding predictions and is expected, at convergence, to follow a zero-mean Gaussian distribution. This condition cannot be satisfied when the observations are biased; therefore, accounting for such biases requires a non-standard, bias-aware implementation.

2.3. **Ensemble Kalman filter.** The EnKF is a MC approximation of the KF that uses an ensemble of N_p particles to represent the state distribution. Each particle is propagated through the transition model, and the ensemble statistics are used to compute the moments of the state distribution:

$$\boldsymbol{x} \approx \bar{\boldsymbol{x}} \doteq \frac{1}{N_p}\sum_{i=1}^{N_p}\boldsymbol{x}_i, \quad \boldsymbol{P} \approx \boldsymbol{S} \doteq \frac{1}{N_p - 1}\sum_{i=1}^{N_p}(\boldsymbol{x}_i - \bar{\boldsymbol{x}})(\boldsymbol{x}_i - \bar{\boldsymbol{x}})^T.$$

There are several variants of the EnKF, which differ in how they implement the analysis step. Here, we recall arguably the most frequently used one – the stochastic EnKF – and refer to [34] for the deterministic ensemble Kalman filter (DEnKF) and to [35] for the square-root EnKF. Once again dropping the time index for simplicity, the analysis of the stochastic EnKF reads as follows:

$$\boldsymbol{x}_a^{(i)} = \boldsymbol{x}_f^{(i)} + \boldsymbol{K}\left(\boldsymbol{u}_{\text{obs}}^{(i)} - \boldsymbol{H}\boldsymbol{x}_f^{(i)}\right), \qquad \boldsymbol{u}_{\text{obs}}^{(i)} \doteq \boldsymbol{u}_{\text{obs}} + \boldsymbol{\sigma}^{(i)}, \qquad i = 1, \ldots, N_p, \tag{7}$$

where $\boldsymbol{\sigma}^{(i)}$ is a realisation of the observation noise, i.e. $\boldsymbol{\sigma}^{(i)} \sim \mathcal{N}(\boldsymbol{0}, \boldsymbol{\Sigma})$. This perturbation of the observation is a key feature of the stochastic EnKF, and aims to avoid the underestimation of the analysis covariance [36], a common issue

[1]This is the so-called Gaussian assumption, which assumes (i) Gaussianity of the noise, (ii) Gaussianity of the initial guess, i.e. $\boldsymbol{x}_a^0$, and (iii) that the transition operator is "linear enough" so that it preserves the Gaussianity of the input.

in ensemble-based methods. The Kalman gain $\boldsymbol{K}$ is computed as in (6), with $\boldsymbol{P}_f\boldsymbol{H}^T$ and $\boldsymbol{H}\boldsymbol{P}_f\boldsymbol{H}^T$ replaced by their ensemble counterparts:

$$\boldsymbol{P}_f\boldsymbol{H}^T \equiv \frac{1}{N_p-1}\sum_{i=1}^{N_p}(\boldsymbol{x}_f^{(i)}-\bar{\boldsymbol{x}}_f)(\boldsymbol{y}^{(i)}-\bar{\boldsymbol{y}})^T, \qquad \boldsymbol{H}\boldsymbol{P}_f\boldsymbol{H}^T \equiv \frac{1}{N_p-1}\sum_{i=1}^{N_p}(\boldsymbol{y}^{(i)}-\bar{\boldsymbol{y}})(\boldsymbol{y}^{(i)}-\bar{\boldsymbol{y}})^T,$$

where $\boldsymbol{y}^{(i)} \doteq \boldsymbol{H}\boldsymbol{x}_f^{(i)}$ is the predicted observation for the i-th particle. Crucially, $\boldsymbol{P}_f$ is never formed explicitly, so the analysis costs $\mathcal{O}(N_pN_xN_{\text{obs}})$ per cycle rather than $\mathcal{O}(N_x^3)$, a significant saving whenever $N_p \ll N_x$. The EnKF is also asymptotically consistent: in the limit $N_p \to \infty$, its solution converges to the optimal one, even for nonlinear dynamics [35]. In practice, N_p is kept far below N_x, and accuracy at small ensemble sizes is recovered through inflation [20, 37], localisation [20, 38], and adaptivity [21], which are discussed in the next subsection.

2.4. **Auxiliary EnKF methodologies: inflation, localisation, and adaptivity.** A well-known pathology of the EnKF is that $\boldsymbol{S}$, being a finite-sample estimate of $\boldsymbol{P}$ built from only $N_p \ll N_x$ members, systematically underestimates the true forecast spread, which may cause the ensemble to collapse around a (potentially biased) estimate and stop responding to observations. Multiplicative covariance inflation [37] is the simplest remedy: before the analysis step, every forecast deviation from the ensemble mean is rescaled by a factor $\rho > 1$,

$$\boldsymbol{x}_f^{(i)} \leftarrow \bar{\boldsymbol{x}}_f + \rho\left(\boldsymbol{x}_f^{(i)} - \bar{\boldsymbol{x}}_f\right), \qquad i = 1,\dots,N_p,$$

which leaves the ensemble mean unchanged while inflating the sample covariance by ρ^2, i.e. $\boldsymbol{S}_f \leftarrow \rho^2\boldsymbol{S}_f$. More advanced methods in the literature consider time-varying inflation factors, for example the one developed in [20]. Here, the authors estimate a new value of ρ at every cycle, together with a localisation of the ensemble covariance, directly from the data. Localisation techniques have been proposed to dampen spurious long-range correlations that are sometimes visible in $\boldsymbol{S}_f$ due to the finite ensemble size [19]. Usually, they replace $\boldsymbol{S}_f$ by a localised version $\boldsymbol{\mathcal{L}} \circ \boldsymbol{S}_f$, where $\boldsymbol{\mathcal{L}}$ is a distance-based correlation-tapering operator (e.g. of Gaspari–Cohn type [39]). In Opals, we implement the following iterative updates, proposed in [20]:

(1) Estimate $\boldsymbol{\mathcal{L}}$ by choosing a length scale such that the resulting localised covariance is consistent with the original $\boldsymbol{S}_f$.
(2) Estimate ρ as the maximum likelihood estimate (MLE) of an inflated, localised version of (7), which amounts to minimising

$$\text{NLL}(\rho) \doteq \frac{1}{2}\boldsymbol{d}^T\boldsymbol{C}(\rho)^{-1}\boldsymbol{d} + \frac{1}{2}\log\det\boldsymbol{C}(\rho), \qquad \boldsymbol{C}(\rho) \doteq \rho^2\boldsymbol{H}\left(\boldsymbol{\mathcal{L}} \circ \boldsymbol{S}_f\right)\boldsymbol{H}^T + \boldsymbol{\Sigma}.$$

Finally, [21] addresses a complementary problem: rather than explicitly adjusting the ensemble spread, optimal values for the noise covariances $\boldsymbol{\Pi}$ and $\boldsymbol{\Sigma}$ are adaptively sought to recover the optimality of the filter, as detailed in [40]. The authors have likened this approach to a form of *additive* inflation, as opposed to the multiplicative inflation discussed earlier. In practice, this lets $\boldsymbol{\Pi}$ and $\boldsymbol{\Sigma}$ track genuine changes in model or instrument error over the course of an experiment, rather than remaining fixed at whatever values were assumed at initialisation – which is the default procedure in standard KFs.

2.5. **Bias-aware Kalman filters.** Bias-aware KFs are a class of methods that explicitly account for systematic errors in the filtering procedure, usually by including a bias term in the observation space. A sizeable portion of Opals is dedicated to bias-aware implementations, largely following the approaches in [23, 41][2]. In particular, the latter reference employs a bias-aware observation operator of the form (2), and seeks to minimise

$$\mathcal{L}_{\text{BA-KF}}(\boldsymbol{x}) \doteq \mathcal{L}_{\text{KF}}(\boldsymbol{x}) + \frac{\gamma}{2}\|\boldsymbol{b}\|^2_{\boldsymbol{\Xi}^{-1}}, \tag{8}$$

where $\gamma \geq 0$ is a regularisation parameter and $\boldsymbol{\Xi} \in \mathbb{R}^{N_{\text{obs}}\times N_{\text{obs}}}$ is a covariance matrix for the bias, commonly chosen as $\boldsymbol{\Xi} \equiv \boldsymbol{\Sigma}$. The analysis step and the expression of the Kalman gain are then modified to minimise (8):

$$\begin{aligned}\boldsymbol{x}_a &= \boldsymbol{x}_f + \boldsymbol{K}\left((\boldsymbol{I}+\boldsymbol{J})(\boldsymbol{u}_{\text{obs}} - \boldsymbol{H}\boldsymbol{x}_f - \boldsymbol{b}) - \gamma\boldsymbol{\Sigma}\boldsymbol{\Xi}^{-1}\boldsymbol{J}\boldsymbol{b}\right),\\ \boldsymbol{K} &\doteq \boldsymbol{P}_f\boldsymbol{H}^T\left(\left((\boldsymbol{I}+\boldsymbol{J})(\boldsymbol{I}+\boldsymbol{J})^T + \gamma\boldsymbol{\Sigma}\boldsymbol{\Xi}^{-1}\boldsymbol{J}\boldsymbol{J}^T\right)\boldsymbol{H}\boldsymbol{P}_f\boldsymbol{H}^T + \boldsymbol{\Sigma}\right)^{-1},\end{aligned} \tag{9}$$

where $\boldsymbol{J} \doteq \frac{\partial \boldsymbol{b}}{\partial(\boldsymbol{H}\boldsymbol{x}_f)}$. Specifically, in [23], the authors model the bias with an echo state network (ESN) [42], which is a recurrent neural network with a sparsely connected hidden layer with random entries. In [23], the authors argue for the great suitability of ESNs in the context of bias modelling for KF pipelines, given (i) their ability to capture time-evolving processes [41], (ii) their relatively low computational cost (also for training), and (iii) the straightforward computation of $\boldsymbol{J}$. We recall that a standard ESN at the kth time step may be formulated as

$$\boldsymbol{b}^k(\boldsymbol{y}) = \boldsymbol{W}_{\text{out}}\boldsymbol{r}^k(\boldsymbol{y}), \quad \boldsymbol{r}^k(\boldsymbol{y}) = (1-\alpha)\boldsymbol{r}^{k-1}(\boldsymbol{y}) + \alpha f(\boldsymbol{W}_{\text{in}}\boldsymbol{y}^k + \boldsymbol{W}_{\text{hid}}\boldsymbol{r}^{k-1}), \qquad \boldsymbol{r}^k \in \mathbb{R}^{N_r},\ \boldsymbol{y}^k \in \mathbb{R}^{N_{\text{obs}}}, \tag{10}$$

where $\alpha \in [0,1]$, f is the activation function (usually a hyperbolic tangent), the matrices $\boldsymbol{W}_{\text{in}} \in \mathbb{R}^{N_r\times N_{\text{obs}}}$ and $\boldsymbol{W}_{\text{hid}} \in \mathbb{R}^{N_r\times N_r}$ are two fixed matrices, $\boldsymbol{W}_{\text{out}} \in \mathbb{R}^{N_{\text{obs}}\times N_r}$ is the only trainable parameter of the network, $\boldsymbol{r}$ is the so-called

[2]We note that these references discuss the specific case of a bias-aware EnKF. However, as we believe the principles can be extended to other filter variants, the present subsection employs a broader perspective than our references.

Algorithm 1 Bias-aware Kalman filter

Initialise training data: $(\boldsymbol{R}, \boldsymbol{B}) = ([], [])$ ▷ ESN training
for $k = 1 : N_{\text{train}}$ **do**
  Run transition: $\left(\boldsymbol{x}^k, \boldsymbol{b}^k\right) = \left(\boldsymbol{\mathcal{F}}_{\boldsymbol{\theta}}(\boldsymbol{x}^{k-1}), \boldsymbol{u}^k_{\text{obs}} - \boldsymbol{H}\boldsymbol{x}^k\right)$
  Accumulate training data: $(\boldsymbol{R}, \boldsymbol{B}) \leftarrow \left([\boldsymbol{R}, \boldsymbol{r}^k(\boldsymbol{b}^k)], [\boldsymbol{B}, \boldsymbol{b}^k]\right)$
end for
Train ESN with ridge regression (11)
for $k = N_{\text{train}} + 1 : N_{\text{train}} + N_{\text{wash}}$ **do** ▷ ESN washout
  Run transition: $\left(\boldsymbol{x}^k, \boldsymbol{b}^k\right) = \left(\boldsymbol{\mathcal{F}}_{\boldsymbol{\theta}}(\boldsymbol{x}^{k-1}), \boldsymbol{u}^k_{\text{obs}} - \boldsymbol{H}\boldsymbol{x}^k\right)$
  Update hidden state (10): $\boldsymbol{r}^k = \boldsymbol{r}^k(\boldsymbol{b}^{k-1})$
end for
for $k = N_{\text{train}} + N_{\text{wash}} + 1 : N_{\text{train}} + N_{\text{wash}} + N_t$ **do** ▷ Bias-aware DA
  Run ESN in closed-loop: $\left(\boldsymbol{r}^k, \boldsymbol{b}^k\right) = \left(\boldsymbol{r}^k(\boldsymbol{b}^{k-1}), \boldsymbol{W}_{\text{out}}\boldsymbol{r}^k(\boldsymbol{b}^{k-1})\right)$
  Compute $\boldsymbol{J}$ as outlined in [23]
  Run transition: $\boldsymbol{x}^k_f = \boldsymbol{\mathcal{F}}_{\boldsymbol{\theta}}(\boldsymbol{x}^{k-1}_a)$
  Run analysis (9)
end for

hidden state, $\boldsymbol{y}$ is the input to the network, and $\boldsymbol{b}$ is clearly the output. For the precise formulation of the ESN employed throughout this work, we refer to [23], which considers a more complex formulation than that in Eq. (10). There are two possible configurations for the ESN:

- *open-loop*: the input variable is set to a given (training) value. This configuration is used during the training phase.
- *closed-loop*: the input variable is set to the previous output of the network, that is $\boldsymbol{y}^k \doteq \boldsymbol{b}^{k-1}$. This configuration is used whenever we wish to evaluate the ESN – i.e. the bias model – once it is trained.

The reason why training an ESN is inexpensive is that it reduces to a ridge regression problem [43]

$$\boldsymbol{W}_{\text{out}} = \arg\min_{\boldsymbol{W}} \sum_{k=1}^{N_{\text{train}}} \left\|\boldsymbol{b}^k - \boldsymbol{W}\boldsymbol{r}^k(\boldsymbol{y})\right\|_2^2 + \lambda\|\boldsymbol{W}\|_2^2 \implies \boldsymbol{W}_{\text{out}} = \boldsymbol{B}\boldsymbol{R}^T(\boldsymbol{R}\boldsymbol{R}^T + \lambda\boldsymbol{I})^{-1}, \tag{11}$$

which is far more efficient than backpropagation with gradient descent methods. In Eq. (11), $\lambda \geq 0$ represents the Tikhonov regularisation parameter, whereas $\boldsymbol{B} \in \mathbb{R}^{N_{\text{obs}} \times N_{\text{train}}}$ is a matrix of training biases (obtained by concatenating N_{train} observed biases during the training phase) and $\boldsymbol{R} \in \mathbb{R}^{N_r \times N_{\text{train}}}$ is a matrix of training hidden states (obtained by running (10) in closed-loop on the observed biases).
Although several considerations have been omitted in the present work for brevity, the overall procedure for constructing and running a bias-aware KF is summarised in Alg. 1. For a detailed explanation, we refer to the original work [23].

2.6. **Incorporating reduced error models into the Kalman filter.** When the transition model $\boldsymbol{\mathcal{A}}_{\boldsymbol{\theta}}$ is replaced by a computationally cheaper surrogate – e.g. a ROM [44–48] – to make repeated evaluations within the DA pipeline tractable, an appropriate filtering technique is needed to account for the resulting surrogate error. While this could in principle be handled by the bias-aware filter of Subsection 2.5, the ROM error is more naturally treated as a zero-mean, parameter-dependent quantity that is small near the training samples and grows predictably away from them. To this end, we adopt the approach of [22], though we note that this is more a working choice than a definitive strategy, since identifying the most suitable strategy for surrogate-error-aware DA remains an open question we intend to keep exploring. However, the latter already provides a practical, computationally inexpensive framework for the problems considered here.

The approach proposed in [22] can be briefly summarised as follows:

(1) A dictionary of FE solutions $\{\boldsymbol{u}^k(\boldsymbol{\mu}_i)\}_i^{N_{\text{train}}}$ – with $k = 1, \ldots, N_t$ – is generated at a set of training parameters $\{\boldsymbol{\mu}_i\}_{i=1}^{N_{\text{train}}}$. Of these, a number $N_{\text{off}} \leq N_{\text{train}}$ of offline parameters are used to construct an n-dimensional ROM subspace $\text{span}\{\boldsymbol{\phi}_i\}_{i=1}^n \subset \mathbb{R}^{N_u}$, with $n \ll N_u$, such that

$$\frac{d\widehat{\boldsymbol{u}}(\boldsymbol{\mu})}{dt} + \widehat{\boldsymbol{\mathcal{A}}}(\widehat{\boldsymbol{u}}(\boldsymbol{\mu}); \boldsymbol{\mu}) = \boldsymbol{0}, \quad \text{where hopefully } \boldsymbol{u}_n(\boldsymbol{\mu}) \doteq \sum_{i=1}^n \widehat{u}_i(\boldsymbol{\mu})\boldsymbol{\phi}_i \approx \boldsymbol{u}(\boldsymbol{\mu}) \;\; \forall \boldsymbol{\mu} \in \{\boldsymbol{\mu}_i\}_{i=1}^{N_{\text{off}}}. \tag{12}$$

For a complete review of the ROM methodologies used to derive Eq. (12), we refer to the "classics" [44, 45], as well as to our works [46–48], and to [25], which describes the implementation details of GridapROMs.jl, our in-house ROM Julia library that we exploit for the practical computation of ROMs.

(2) We consider a biased observation operator as in (2), with the bias term being the ROM error, i.e.

$$\boldsymbol{b} \equiv \boldsymbol{b}(\boldsymbol{\mu}) \doteq \boldsymbol{G}\left(\boldsymbol{u}(\boldsymbol{\mu}) - \boldsymbol{u}_n(\boldsymbol{\mu})\right).$$

In practice, as the value of $\boldsymbol{\mu}$ is unknown, $\boldsymbol{b}$ needs to be efficiently estimated across the entire parameter space. To this end, [22] consider the best linear unbiased prediction (BLUP) associated with the random process $\{\boldsymbol{b}(\boldsymbol{\mu}_i)\}_{i=1}^{N_{\text{cal}}}$,

with $N_{\text{cal}} \leq N_{\text{train}}$ being the number of calibration parameters, obtained via kriging-based interpolation [49]. In essence, the BLUP – here referred to as $\boldsymbol{\beta}$ – is computed as a linear combination of the bias at the calibration parameters:

$$\boldsymbol{\beta}(\boldsymbol{\mu}) \doteq \sum_{i=1}^{N_{\text{cal}}} w_i(\boldsymbol{\mu})\boldsymbol{b}(\boldsymbol{\mu}_i),$$

where $\{w_i\}_{i=1}^{N_{\text{cal}}}$ are the kriging weights found by solving a constrained optimisation problem – minimisation of the variance of $\boldsymbol{\beta} - \boldsymbol{b}$, while imposing $\boldsymbol{\beta}$ to be zero-mean – over the set of calibration parameters [22].

The analysis step and the expression of the Kalman gain of a standard KF are modified as follows:

$$\boldsymbol{x}_a = \boldsymbol{x}_f + \boldsymbol{K}\left(\boldsymbol{u}_{\text{obs}} - \boldsymbol{H}\boldsymbol{x}_f - \boldsymbol{\beta}\right), \qquad \boldsymbol{K} \doteq \boldsymbol{P}_f\boldsymbol{H}^T\left(\boldsymbol{H}\boldsymbol{P}_f\boldsymbol{H}^T + \boldsymbol{\Sigma} + \boldsymbol{\Gamma}\right)^{-1}, \tag{13}$$

where $\boldsymbol{\Gamma}$ is the matrix of trace variances associated with $\boldsymbol{\beta}$ [22]. Overall, this approach is easily incorporated within a KF pipeline, since it only requires minor modifications to Eq. (13). The approach is computationally inexpensive, since the ROM training and the kriging weights computation are performed during the offline phase, assuming that $N_{\text{cal}} \approx N_{\text{off}}$, so that the number of required snapshots N_{train} is limited. We also note that rigorous *a priori* error bounds for the ROM have been used in the literature [7] for the same purpose, but strong assumptions on the formulation of the PDE are required. Another approach that we may consider in the future is to estimate the bias term $\boldsymbol{b}$ directly from the ROM residual.

2.7. **Other Bayesian methods: unscented Kalman filter and particle filters.** For completeness, we close this section with a brief overview of the remaining methodologies implemented in Opals. So far, we have mentioned the EKF (linearisation of operators) and EnKF (MC approximation) as ways to handle potential nonlinearity in the system. The UKF [50, 51] uses a different approach to achieve the same goal: it propagates a small, deterministic set of *sigma points* through the nonlinear map $\boldsymbol{\mathcal{F}}_{\boldsymbol{\theta}}$, and reconstructs $\boldsymbol{x}_f$ and $\boldsymbol{P}_f$ from the transformed points. This captures the effect of nonlinearity on the first two moments to a higher order than the EKF linearisation, at a comparable cost, while the analysis step itself remains unchanged from Eq. (6).

Despite sharing many similarities with KFs (particularly the EnKF), particle filters dispense with the Gaussian assumption entirely, representing $p(\boldsymbol{x} \mid \boldsymbol{u}_{\text{obs}})$ by a weighted sample $\{\boldsymbol{x}^{(i)}, w^{(i)}\}_{i=1}^{N_p}$ rather than by its first two moments. Weights are updated multiplicatively with the observation likelihood, $w^{(i)} \propto w^{(i)}\, p(\boldsymbol{u}_{\text{obs}} \mid \boldsymbol{x}_f^{(i)})$, and the particles are periodically resampled to counteract *weight degeneracy*, the well-known tendency of all but a few weights to collapse to zero. Opals implements sequential importance resampling (SIR) and the regularised particle filter discussed in [33]. We finally recall that no linearity assumption is placed on $\boldsymbol{\mathcal{A}}_{\boldsymbol{\theta}}$ or $\boldsymbol{\mathcal{G}}_{\boldsymbol{\sigma}}$, and that particle filters are asymptotically exact as $N_p \to \infty$.

2.8. **Variational methods.** Variational DA methods recast the state-parameter estimation problem as a gradient-based optimisation procedure. In essence, a trajectory $\{\boldsymbol{x}^k\}_k$ is sought to minimise, over a given time window, a cost function measuring the discrepancy between:

- The available observations and the predicted observations obtained by applying the observation operator to the trajectory, i.e. $\boldsymbol{\mathcal{H}}(\boldsymbol{x}^k)$.
- The trajectory's initial state and a background estimate, which represents our prior knowledge about the system.

We tackle two common formulations. First, the 4D-Var [11] seeks an initial condition whose model trajectory provides the best fit to observations distributed over the entire assimilation window (t^0, T), that is

$$\mathcal{L}_{\text{4d-var}}(\boldsymbol{x}^0) \doteq \frac{1}{2}\|\boldsymbol{x}^0 - \boldsymbol{x}_b\|^2_{\boldsymbol{B}^{-1}} + \frac{1}{2}\sum_{k=1}^{N_t}\|\boldsymbol{u}^k_{\text{obs}} - \boldsymbol{\mathcal{H}}\left(\boldsymbol{x}^k\right)\|^2_{\boldsymbol{\Sigma}^{-1}}, \quad \text{where } \boldsymbol{x}^k = \boldsymbol{\mathcal{F}}(\boldsymbol{x}^{k-1}), \tag{14}$$

where $\boldsymbol{x}_b \in \mathbb{R}^{N_x}$ is the aforementioned background estimate, and $\boldsymbol{B} \in \mathbb{R}^{N_x \times N_x}$ is its associated covariance. Second, the 3D-Var [10] iteratively seeks an estimate of the state at one single time step at the time:

$$\mathcal{L}_{\text{3d-var}}(\boldsymbol{x}^0) \doteq \frac{1}{2}\|\boldsymbol{x}^0 - \boldsymbol{x}_b\|^2_{\boldsymbol{B}^{-1}} + \frac{1}{2}\|\boldsymbol{u}^k_{\text{obs}} - \boldsymbol{\mathcal{H}}\left(\boldsymbol{x}^k\right)\|^2_{\boldsymbol{\Sigma}^{-1}}, \quad \text{where } \boldsymbol{x}^k = \boldsymbol{\mathcal{F}}(\boldsymbol{x}^{k-1}), \quad k = 1, \ldots, N_t. \tag{15}$$

After each optimisation step, the value of the background estimate is updated to the solution obtained at the previous time step, that is $\boldsymbol{x}_b \leftarrow \boldsymbol{x}^{k-1}$ for every $k \geq 2$. The minimisation of Eqs. (14)-(15) is performed very efficiently in Opals, by exploiting the automatic differentiation capabilities of the packages SciMLSensitivity [16] and GridapTopOpt.jl [52] for ODEs and PDEs, respectively, to compute the loss gradients. The ensuing gradient descent-like minimisation procedure is then performed with the BFGS algorithm [53].

Remark 1. *Though not apparent from Eq.* (14)*, the 4D-Var in general still operates sequentially as most DA strategies. Indeed, once new observations become available past T, the 4D-Var is re-run over a new assimilation window, with the initial condition set to the previously estimated $\boldsymbol{x}^{N_t}$ from* (14)*.*

Abstract type	Purpose
`Law`	Probabilistic representation of state/parameter variables
`Model`	Forward/observation operators (e.g. custom linear/nonlinear maps, SciML ODEs, Gridap PDEs)
`DAMethod`	Abstraction shared by DA methods

TABLE 1. Main abstract types involved in Opals.

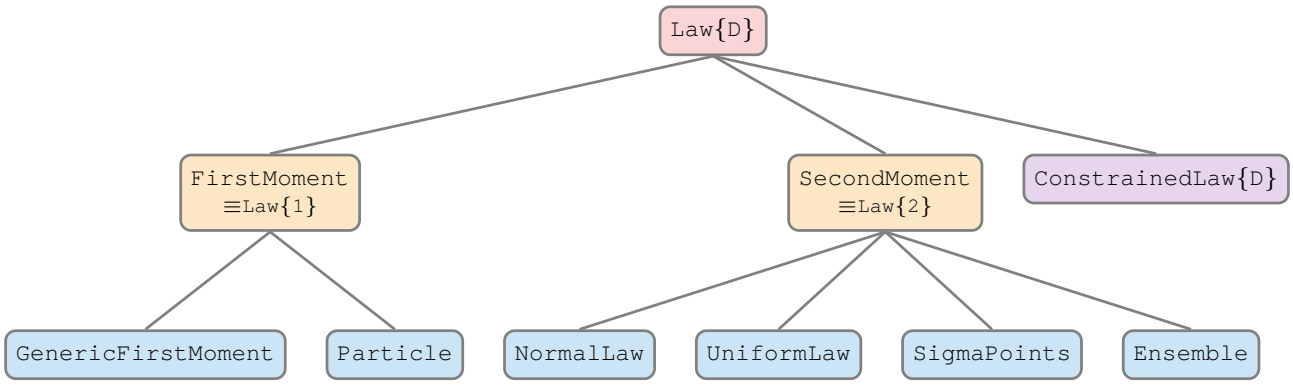

FIGURE 2. `Law` hierarchy. In red: abstract types; in orange: type aliases; in purple: parametric subtypes; and in blue: concrete subtypes.

3. IMPLEMENTATION DETAILS

This section describes how the methodologies of Subsection 2 are realised in code. Subsection 3.1 introduces the main abstractions around which the whole package is organised. Subsection 3.2 details the native interoperability layer with the SciML and Gridap/GridapROMs ecosystems, through which an arbitrary ODE or transient, full- or reduced-order PDE solution can serve as a transition model with no change to the surrounding assimilation code. Subsection 3.3 presents the high-level API used to assemble a complete DA experiment, and Subsection 3.4 describes the self-contained, cache-efficient RC implementation underlying the bias-aware filter of Subsection 2.5. The section closes, in Subsection 3.5, with a complete usage example.
Since most implementation efforts in Opals are devoted to Bayesian filtering techniques, rather than variational methods, we focus most of our attention on the former in this section. In any case, the latter are implemented in a similar fashion, and the interested reader is referred to the source code for further details.

3.1. **Types and hierarchy.** A considerable portion of Opals is organised around a small number of abstract types, summarised in Table 1. A `Law` is an interface for probability distributions of parameters and states that can be efficiently propagated through a `Model`, which in general represents any map, and is mostly used to describe a transition or observation operator. The `Law` hierarchy is shown in Figure 2. The leaves of the tree (i.e. concrete types) are the distributions used throughout the methods described in Section 2: a `NormalLaw` is the default type for the prior propagated throughout a KF and for the representation of noise distributions, `Ensemble` is an ensemble law used for EnKFs, and similarly `SigmaPoints`, `Particle` and `GenericFirstMoment` are respectively used for UKFs, particle filters, and variational methods. The last distribution we mention is the `ConstrainedLaw`, which wraps a `Law` and a set of constraints that are used to enforce bounds on the state variables after propagation. This is useful, for instance, when the unknown parameters are known to belong to a certain parameter space.

The `Model` hierarchy in Figure 3 shows how these types are categorised depending on whether they represent a linear map (`LinearModel`) or a nonlinear one (`NonlinearModel`). For the former, the most important example is the `AlgebraicModel`, which simply wraps the matrix; for the latter, we mention (i) the `TaperModel`, which represents the tapering operator $\mathcal{L}$ discussed in Subsection 2.4, (ii) the `ODEModel` and `TransientPDEModel` used whenever the transition is defined by ODEs and transient PDEs, and (iii) the `GenericModel`, which wraps a generic Julia function (or a Gridap `Map` [24]). Another notable subtype is the `MemoryModel`, which wraps a `Model` and a `Law`; we will clarify the usefulness of the latter in Section 4.
The user may think of a `Model` as an efficient `Law`-to-`Law` map (although it also works as an `AbstractArray`-to-`AbstractArray` mapping). The efficiency is driven by a cache-friendly design, which allows the user to preallocate any buffer needed for its evaluation and then reuse it in every subsequent call. This clearly separates the `Model` from a plain Julia function, and is a crucial design choice in the context of DA, where the transition and observation operators are evaluated repeatedly in a loop, often over an ensemble of states. The system of caches is implemented following a similar

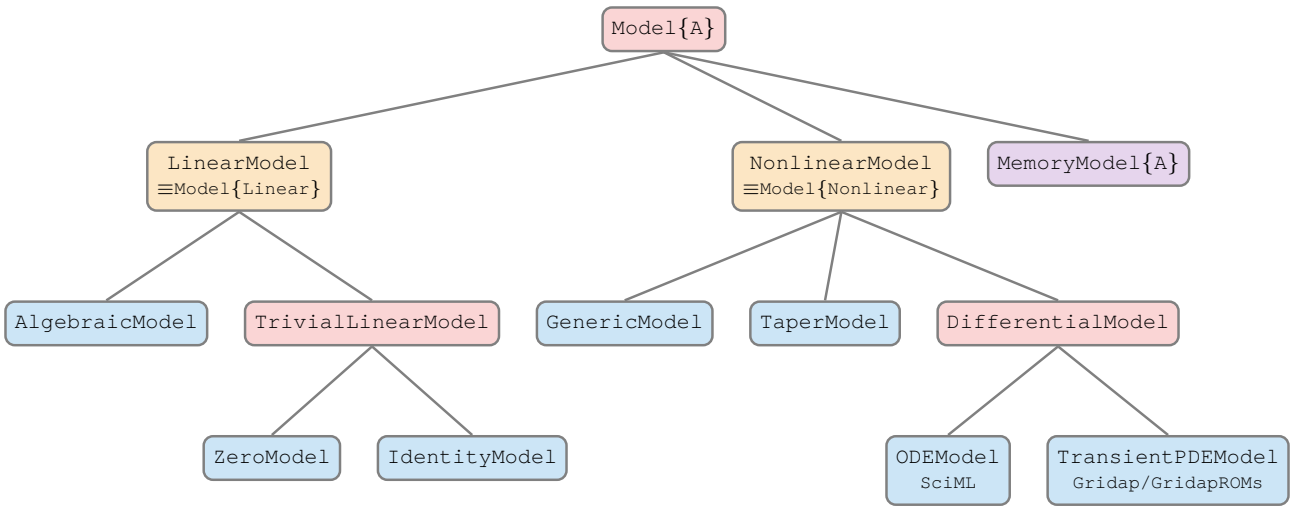

FIGURE 3. `Model` hierarchy. In red: abstract types; in orange: type aliases; in purple: parametric subtypes; and in blue: concrete subtypes.

filter_loop.jl

```julia
function evaluate!(
  posterior::Law,
  f::Filter,
  args...
  )

  forecast!(posterior,f)
  analyse!(posterior,f,args...)
  return posterior
end

function loop(
  f::Filter,
  obs::AbstractArray{T,N}
  ) where {T,N}

  prior = get_prior(f)
  posterior = similar_law(prior)
  history = typeof(prior)[]

  for k in axes(obs,N)
    dₖ = selectdim(obs,N,k)
    copyto!(prior,posterior)
    isnan(dₖ) ? evaluate!(posterior,f) :
      evaluate!(posterior,f,dₖ)
    push!(history,copy(posterior))
  end

  return history
end
```

FIGURE 4. Simplified implementation of the DA loop for `Filter` subtypes. Though a similar implementation holds for `VariationalMethod`, the latter dispenses with the forecast-then-analyse paradigm.

design as in Gridap, namely by extending the `return_cache` and `evaluate!` methods implemented therein.

Every one of the methods described throughout Section 2 is implemented either as a `Filter` or as a `VariationalMethod`, both subtypes of a common `DAMethod` abstraction. Conceptually, a `DAMethod` is an object defined by a (transition, observation) `Model` pair, a (prior, observation prior) `Law` pair, a (process noise, observation noise) `Law` pair, a set of methods that implement the forecast and analysis steps, and lastly a cache structure collecting all the necessary buffers to perform these steps in-place. Given a `DAMethod` and some observations, the DA can be launched simply by calling the `loop` method, whose basic implementation is shown in Listing 4. As the name suggests, the latter implements a *for* loop over the observations (assumed to be stacked along their last axis), whereupon the posterior is continuously updated according to the `forecast!` and `analyse!` methods specified for `Filter`s, and via an optimisation on sliding windows for `VariationalMethod`s. A vector of posterior `Law`s – referred to throughout this work as the filter's history – is the output of `loop`. The roles of `forecast!` and `analyse!` can be summarised in Table 2.

The `DAMethod` hierarchy is summarised in Figure 5. The leaves of the tree are the concrete implementations of some of the methods described in Section 2: `KalmanFilter`, `UnscentedKalmanFilter`, `EnsembleKalmanFilter`, and `ParticleFilter` are respectively the implementations of the KF, UKF, EnKF, and particle filter; while `VariationalMethod` constitutes the backbone for our variational methods[3]. The EKF is essentially a `KalmanFilter` – which represents the standard KF as presented in Subsection 2.2 – whose transition and/or observation operators are

[3]We note that 3D-Var and 4D-Var share the same exact structure up to the definition of their respective assimilation windows (see Eqs. (14)-(15)), and thus we do not implement them separately.

Method	Parent method	Purpose	Output
`transition!`	`forecast!`	Runs the transition `Model` on the posterior from the previous time step	$\boldsymbol{x}_f^k = \boldsymbol{\mathcal{F}}_{\boldsymbol{\theta}}(\boldsymbol{x}_a^{k-1})$
`observation!`	`analyse!`	Runs the observation `Model` on the output of `forecast!`	$\boldsymbol{H}\boldsymbol{x}_f^k$
`innovation!`	`analyse!`	Computes the innovation by removing the current observation	$\boldsymbol{u}_{\text{obs}} - \boldsymbol{H}\boldsymbol{x}_f^k$
`kalman_gain!`	`analyse!`	Computes the Kalman gain	$\boldsymbol{K}$
`update!`	`analyse!`	Computes the analysed posterior `Law`	$\boldsymbol{x}_a^k$

TABLE 2. Workflow of `forecast!` and `analyse!`, the two core methods in the `DAMethod` class.

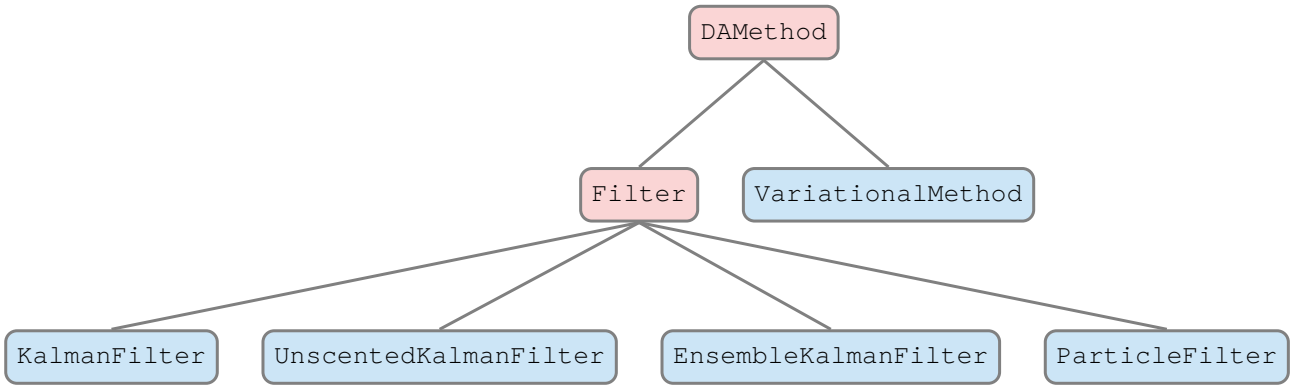

FIGURE 5. `DAMethod` hierarchy. In red: abstract types; and in blue: concrete subtypes.

filter_composition.jl

```julia
# given: kf = KalmanFilter(...)
# given: taper, inflation
# given: esn (pre-trained)

# localisation
f1 = LocalisationKalmanFilter(kf,taper)
# localisation + inflation
f2 = InflationKalmanFilter(f1,inflation)
# localisation + inflation + adaptive
f3 = AdaptiveKalmanFilter(f2;step=0.1)
# localisation + inflation + adaptive + bias-aware
f4 = BiasAwareKalmanFilter(f3,esn;γ=10)
```

FIGURE 6. Examples of composite `Filter`s in Opals.

subtypes of `NonlinearModel`. The remaining methodologies previously discussed – namely localisation, inflation, adaptivity, bias-awareness and ROM calibration – are implemented as composable wrappers around a `Filter` instance. These wrappers are themselves `Filter` subtypes that hold an inner `Filter`, and therefore only need to specialise a small set of methods (usually, just the ones in Table 2). The seamless filter composition and relatively simple type hierarchies allow for a very flexible and modular design, with minimal effort required to implement new methods or combine existing ones. Examples of `Filter` composition are shown in Figure 6.

3.2. **Native integration with the SciML and Gridap ecosystems.** In this subsection, we focus on the specific cases where the transition operator is an ODE or a transient PDE, which comprise a large portion of the applications of interest in the inverse modelling and DA communities. We begin with the former. Arguably the most commonly used package for ODEs in the Julia ecosystem is SciML's OrdinaryDiffEq.jl [54], which implements a wide range of time-stepping algorithms and provides a common interface for their use. The `ODEWrapper` implemented in Opals is a thin wrapper around any OrdinaryDiffEq.jl integrator, and the `Model` constructor dispatches on it to produce a `ODEModel` that can be used as a transition operator in any `DAMethod` described in the previous subsection. We show in Listing 7 the code implementing this design, along with a minimum-working example constructing a KF. The crucial line of code is the 6th of the listing, and the remaining ones are verbatim. A complete usage example involving ODE-based transition operators is discussed in Subsection 3.5. During the `loop` function, the transition operator is advanced using the Tsitouras $5/4$ Runge-Kutta time integrator [55] implemented in OrdinaryDiffEq.jl.

As shown in Listing 8, a very similar design principle also holds for transient PDEs. In this case, the general constructor `Model` (line 9) dispatches to `TransientPDEModel` when provided with an `ODESolution` input (defined at line 8), a Gridap type. Essentially everything works in the same manner as for the ODE case, with the only difference being that `forecast!` propagates the `Law` in time through a FE integrator, assembler, and solver rather than through an ODE counterpart. We note that the syntax of Listing 8 also allows an `ODESolution` object to wrap a ROM generated by

ode.jl

```julia
# given: ode! = ode!(uₜ,u,μ,_)
# given: (μ⁰,u⁰), P⁰::Noise
# given: t⁰:Δt:T

# in-place ODE --> transition model
probl = ODEWrapper(Tsit5(),ode!,u⁰,t⁰:Δt:T,μ⁰)
transition = Model(probl)

observation = Model(I(N_obs))

N_p = dimension(μ⁰)
law_u⁰ = build_prior(u⁰,P⁰)
law_μ⁰ = build_prior(μ⁰,Noise(zeros(N_p,N_p)))
prior = joint_law(law_μ⁰,law_u⁰)

kf = KalmanFilter(transition,observation,prior)
```

FIGURE 7. Defining a `Filter` for an ODE-constrained problem in Opals.

transient_pde.jl

```julia
# given: op = TransientFEOperator(...)
# (alternatively: op = TransientRBOperator(...))
# given: solver = ThetaMethod(...)
# given: (μ⁰,uₕ⁰), P⁰::Noise
# given: t⁰:Δt:T

# transient PDE --> transition model
sol = solve(solver,op,μ⁰,uₕ⁰)
transition = Model(sol)

observation = Model(I(N_obs))

N_p = dimension(μ⁰)
u⁰ = get_free_dof_values(uₕ⁰)
law_u⁰ = build_prior(u⁰,P⁰)
law_μ⁰ = build_prior(μ⁰,Noise(zeros(N_p,N_p)))
prior = joint_law(law_μ⁰,law_u⁰)

kf = KalmanFilter(transition,observation,prior)
```

FIGURE 8. Defining a `Filter` for a transient PDE-constrained problem in Opals.

high_level_api.jl

```julia
1  # given: kf, true_transition, prior
2  # given: Δt
3
4  ts = TimeStencils(dt=Δt,t0=0.0,t_warmup=5.0,t_da=10.0)
5
6  true_history = execute(true_transition,prior,ts)
7
8  # collect states at the DA times
9  true_states = collect_forecasted_states(true_history[DA])
10
11 # spin up in place on (t0,t_warmup)
12 warmup!(kf,ts)
13
14 # collect observations at the DA times
15 observation = get_observation_model(kf)
16 noise = get_observation_noise(kf)
17 obs = build_observations(observation,true_states,noise)
18
19 results = loop(kf,obs)
20
21 # post-processing
22 visualise(true_states,results)
23 println(RMSE(true_states,results))
```

FIGURE 9. High-level interface in Opals. An instance of `TimeStencils` may be used to define a `StencilArray` representing the history of a transition operator (`true_history`, line 6), which can be lazily indexed as in line 9 and propagated forward in time (line 12). The API also allows for easy construction of observations, observation operators, and running DA.

GridapROMs. This makes it possible to run a computationally cheaper version of the transition operator at each iteration of `loop`, while preserving exactly the same interface and syntax as in Listing 8.

3.3. **High-level interface.** Opals is designed to give the user a simple yet elegant interface for assembling a complete DA experiment without engaging directly with the machinery of Subsection 3.1. This is not a cosmetic convenience: standard experiments typically involve several distinct time intervals – a spin-up window, an assimilation window and, for the bias-aware filter of Subsection 2.5, a training, a washout, and a "spread" window [23] as well – each possibly sampled at a different rate than the observations. We encapsulate this bookkeeping in two structures, `TimeStencils` and `StencilArray`, and expose the resulting workflow through a handful of routines, such as `execute`, `warmup!`, `build_prior`, and `build_observations`, shown in Listing 9. A `TimeStencils` object partitions an experiment into up to six contiguous, named phases – `WARMUP`, `TRAIN`, `WASHOUT`, `SPREAD`, and `DA`, plus `ALL` for the entire window – built by chaining user-supplied durations (`t_warmup`, `t_train`, `t_wash`, `t_spread`, `t_da`) one after another from a starting time `t0`. Each phase is stored as a pair of endpoints and materialised into a concrete time grid on demand: indexing `ts[WARMUP]`, or `ts[TRAIN:SPREAD]` for a contiguous span of phases, returns the corresponding range at the model time step `dt`. Every phase constant has an `OBS`-prefixed counterpart (`OBSWARMUP`, ..., `OBSALL`) denoting the very same interval sampled at the observation time step `dt_obs` instead – the two time scales illustrated in Figure 1 – so that a single

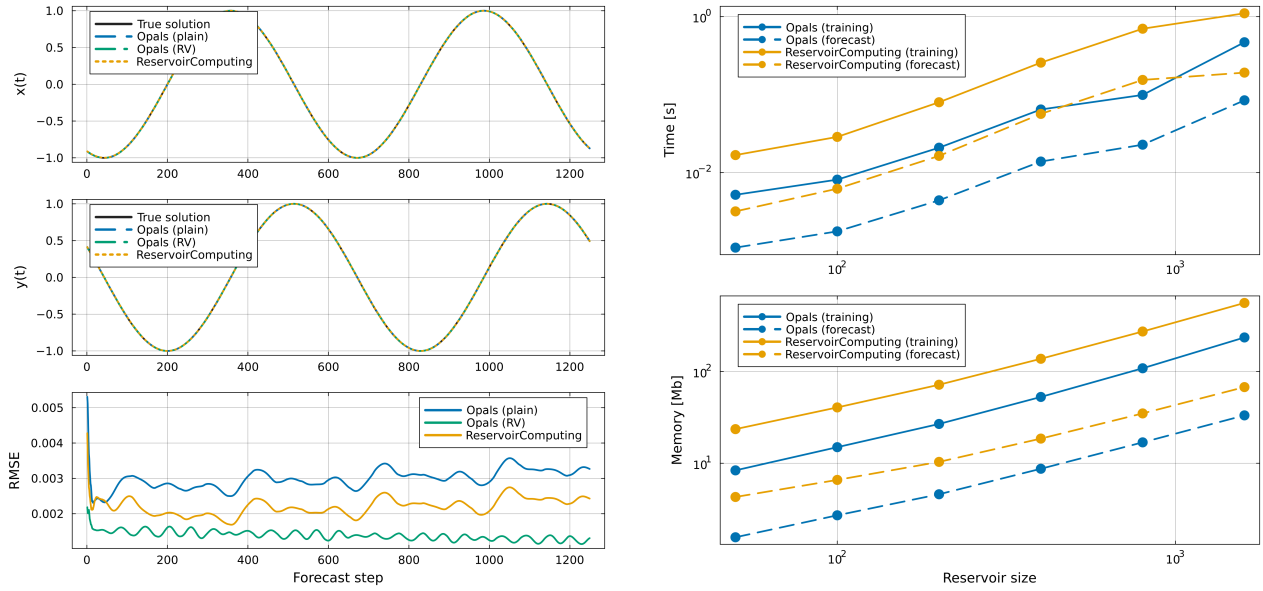

(A) Accuracy (B) Efficiency

FIGURE 10. Comparison of Opals' ESN implementation with ReservoirComputing.jl on the Hopf Bifurcation system [56]. (A) Accuracy comparison in terms of the predicted $x(t)$ and $y(t)$ state coordinates against the true solution, and in terms of RMSE. (B) Efficiency (in terms of time and memory) comparison based on the time required to train the ESN on a training set as a function of the number of hidden units. The results show that Opals' implementation is both more accurate (when using the recycle-validation (RV) strategy) and more efficient than ReservoirComputing.jl. To ensure a fair efficiency comparison, we consider only the plain Opals implementation, since RV training is inherently more computationally expensive, while the forecasting stage is identical in both Opals settings.

`TimeStencils` instance simultaneously drives an integrator at its natural time step and aligns observations to their own, generally coarser, grid.

Rather than having every routine repeat this bookkeeping, `execute` and its relatives return their result wrapped in a `StencilArray`, a lazy container tagging an array with the `TimeStencils` instance and the phase over which it was computed. Re-indexing a `StencilArray` into a different phase does not recompute the trajectory: it calls `restrict` or `expand`, depending on whether the requested phase's grid is coarser or finer than the one currently stored, to resample the time axis of the underlying array onto the new grid. This is what allows, for instance, a full-resolution `WARMUP` trajectory and its coarser `OBSWARMUP` sub-sample to be views of a single computation rather than two separate runs.

More specifically, `execute` runs a transition `Model` forward from a prior `Law` and returns the resulting `StencilArray`; `warmup!` advances a `DAMethod`'s own prior over a phase in-place, discarding the trajectory, which is the idiomatic way to spin up an ODE/PDE integrator (an analogous syntax may be employed for a `EchoStateNetwork`, a type discussed in the next subsection); `build_prior` constructs the initial `Law` appropriate to the target filter from a seed state and covariance; and `build_observations` applies an observation `Model` to a state history to produce synthetic or real observations, optionally corrupted by noise or an additive bias term. Once a `DAMethod` and an observation array are available, `loop` runs the assimilation and returns a `DAResults` object, on which `visualise` and a small library of diagnostics – RMSE, normalised RMSE, negative log-likelihood, the NEES/NIS consistency scores, spread-skill ratio, innovation autocorrelation, and rank histograms – operate directly.

3.4. **Efficient reservoir computing.** The ESN bias model described in Subsection 2.5 is implemented from scratch, rather than by relying on ReservoirComputing.jl [57] – arguably the most widely used RC library in the Julia ecosystem. Opals does reuse two of its utility routines for the initialisation of the fixed weights $\boldsymbol{W}_{\text{in}}$ and $\boldsymbol{W}_{\text{hid}}$ (10), but the forward pass, the ridge-regression training (11), and, more generally, the type hierarchy are a self-contained implementation built around the same caching paradigm discussed in Subsection 3.1 for `Model` subtypes. This improves the efficiency of the models implemented in ReservoirComputing.jl, as shown in Fig. 10. Additionally, a major contribution with respect to ReservoirComputing.jl is the possibility of training the ESN with the *recycle-validation* strategy proposed in [23] for the training of a more accurate bias model. We stress that these are architectural choices motivated by the specific repeated-evaluation setting of the previously discussed bias-aware filtering, and our implementation does not represent a general-purpose substitute for ReservoirComputing.jl, which supports a broader range of RC architectures and training strategies.

lorenz_63.jl

```julia
1 using BlockArrays
2 using GridapROMs
3 using LinearAlgebra
4 using Opals
5 using OrdinaryDiffEq
6 using Statistics
7
8 function lorenz63!(dx,x,p,t)
9     σ,ρ,β = p
10     dx[1] = σ*(x[2]-x[1])
11     dx[2] = x[1]*(ρ-x[3]) - x[2]
12     dx[3] = x[1]*x[2] - β*x[3]
13 end
14
15 # Time and parameter specifications
16 ts = TimeStencils(
17     dt=0.01,t0=0.0,
18     t_warmup=5,t_spread=2,t_da=5
19 )
20 pspace = ParamSpace([[7.0,13.0],[22.0,34.0],[1.5,3.5]])
21
22 # True model
23 N_p = 3
24 N_u = 3
25 true_μ = Realisation([[10.0,28.0,8/3]])
26 true_u⁰    = ParamArray([[1.0,1.0,1.0]])
27 true_probl = ODEWrapper(
28     Tsit5(),lorenz63!,true_u⁰,ts[ALL],true_μ
29 )
30 true_transition = Model(true_probl)
31 true_history = execute(true_transition,ts)
32 true_states = collect_forecasted_states(true_history[DA])
33
34 # Observation model
35 σ_obs = 0.1
36 obs_noise = Noise(σ_obs^2 * I(1))
37 observation = build_linear_observation_model(
38     1:(N_p+N_u),[N_p+1]
39 )
40 obs = build_observations(
41     observation,true_states,obs_noise
42 )
43
44 # Build prior
45 sample_state = collect_forecasted_state(
46     true_history[WARMUP]
47 )
48 init_cov_p = Noise(Diagonal([1.0,2.0,0.3].^2))
49 init_cov_u = Noise(Diagonal([0.2,0.2,0.2].^2))
50 init_cov = joint_law(init_cov_p,init_cov_u)
51 constraints = BlockConstraint(
52     ConstrainTo(pspace),NoConstraint()
53 )
54 prior = build_prior(
55     sample_state,init_cov,constraints;nsamples=60
56 )
57
58 # Transition model on DA times
59 μ⁰,u⁰ = state_blocks(prior)
60 probl = ODEWrapper(
61     Tsit5(),lorenz63!,u⁰,ts[SPREAD:DA],μ⁰,pspace
62 )
63 transition = MemoryModel(Model(probl),prior)
64 _ = execute(transition,ts[SPREAD])
65
66 # Stochastic EnKF
67 prior_enkf = copy(prior)
68 enkf = EnsembleKalmanFilter(
69     transition,observation,prior_enkf;obs_noise
70 )
71 results_enkf = loop(enkf,obs)
72
73 # UKF
74 prior_ukf = ConstrainedLaw(SigmaPoints(prior),constraints)
75 ukf = UnscentedKalmanFilter(
76     transition,observation,prior_ukf;obs_noise
77 )
78 results_ukf = loop(ukf,obs)
79
80 # SIR
81 x⁰ = copy(get_state(prior))
82 prior_sir = ConstrainedLaw(Particle(x⁰),constraints)
83 sir = ParticleFilter(
84     transition,observation,prior_sir;obs_noise
85 )
86 results_sir = loop(sir,obs)
87
88 # Variational method
89 μ⁰,u⁰ = blocks(mean(prior))
90 state_map = ODEStateMap(Tsit5(),lorenz63!,u⁰,ts[DA],μ⁰,pspace)
91 state_observation = build_linear_observation_model(
92     1:N_u,[1]
93 )
94 vm = VariationalMethod(
95     state_map,state_observation;obs_noise
96 )
97
98 N_windows = 10
99 windows = equispaced_windows(ts[DA],N_windows)
100 results_vm = loop(vm,obs,prior;windows,iterations=50)
```

FIGURE 11. Solving the Lorenz-63 DA problem with Opals.

3.5. **Usage example.** In this usage example, we solve a joint parameter-state estimation problem based on the Lorenz-63 equations (lines $1-6$) using four DA strategies: (i) the stochastic EnKF, (ii) the UKF, (iii) the SIR particle filter, and (iv) a variational method. The system jointly estimates three parameters alongside three state variables, and the "true" system is assumed to be the classical chaotic regime obtained for $\boldsymbol{\mu} \doteq (10, 28, 8/3)^T$. Let us address point-by-point the implementation highlights of the script:

- A synthetic trajectory is generated by integrating the true model forward in time[4] (line 24) from an initial condition equal to $(1, 1, 1)^T$. At line 25, the states are extracted from the trajectory in the `DA` interval using the high-level function `collect_forecasted_states`.
- The observation operator (defined at lines $30-32$ using `build_linear_observation_operator`) maps the joint six-dimensional parameter-state vector to its fourth entry, i.e. the first state variable u_1; observations are corrupted by Gaussian noise and collected (lines $33-35$).
- An ensemble prior (lines $37-49$) is derived by adding Gaussian noise to the ensemble state at the end of a warmup phase, with parameters constrained to prescribed ranges via `BlockConstraint` (lines $44-46$), whereas the

[4]The `Realisation` and `ParamArray` types used for the parameter and initial condition are native to GridapROMs.

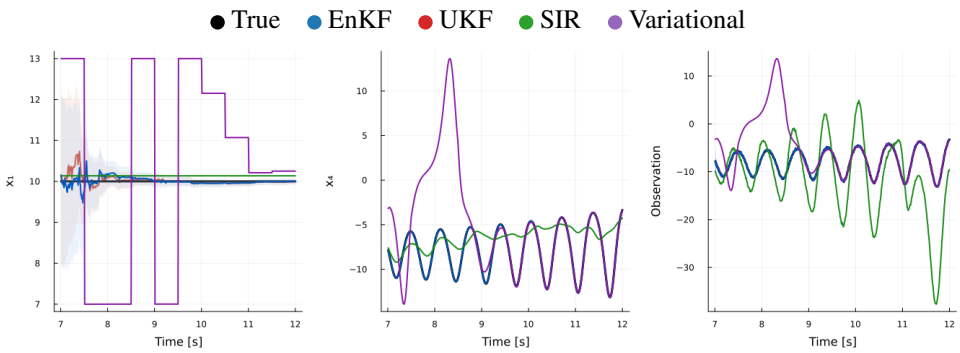

FIGURE 12. Lorenz-63 example. From left to right: (i) estimation of $x_1 \equiv \mu_1$, (ii) estimation of $x_4 \equiv u_1$, and (iii) estimation of observations. We note that, in Opals, the parameter estimate from the variational method is piece-wise constant across each assimilation window.

state variables are unconstrained. The `joint_law` function – called at line 43 – concatenates the two independent noise distributions for $\boldsymbol{\mu}$ and $\boldsymbol{u}$, thus forming a joint distribution.

- The transition model (lines $51 - 57$) is defined as a `MemoryModel` object, initially mentioned in Subsection 3.1. This type is reserved for models which can be idiomatically propagated in time before the start of the DA window, e.g. because they require a warmup phase to be correctly initialised. In this case, the model is propagated over the `SPREAD` window, which is a common practice in order to add sufficient diversity to the ensemble members [34]. The same syntax is used to define the true transition model at line 23, which is used to generate the synthetic observations.
- Lastly, the four DA methods – EnKF (lines $59 - 64$), UKF (lines $66 - 71$), SIR (lines $73 - 79$), and variational (lines $81 - 93$) – are defined and executed. The three Bayesian filters share essentially the same implementation, up to the definition of a different prior `Law` and the choice of the `Filter` subtype. The variational method differs only in that it does not pass a standard transition model, rather it passes an `ODEStateMap` which represents the $\boldsymbol{\mu} \to \boldsymbol{u}$ mapping – needed both for time integration and also to efficiently compute the derivatives of the loss functions (14)-(15) with respect to $\boldsymbol{\mu}$ – and an observation operator defined for the non-augmented state. To run the `loop` for the variational method, in addition to the usual observations, we also need to pass the sliding windows (lines $91 - 92$) and the prior, which represents the background term previously called $\boldsymbol{x}_b$ in Eqs. (14)-(15).

The snippet demonstrates Opals' high-level interface, which allows the user to assemble a complete parameter-state DA experiment – including four different algorithms – with very few lines of expressive code. We underline the central role of `TimeStencils` in order to achieve this. We will present the numerical results of this experiment in Subsection 4.1.

4. NUMERICAL EXAMPLES

In this section, we present four numerical examples that demonstrate the ability of Opals to tackle complex DA problems with a high-level interface while achieving good accuracy. In Subsection 4.1, we report the numerical results obtained from the Lorenz-63 model already discussed in Subsection 3.5. In Subsection 4.2, we construct a `BiasAwareFilter` to solve a Van der Pol oscillator problem with biased observations. In Subsection 4.3, we demonstrate the discovery of the Reynolds number of a turbulent Navier-Stokes flow around a square cavity. Finally, in Subsection 4.4, we showcase DA with model surrogate techniques for the Heat equation, and compare the results obtained with and without the error calibration discussed in Subsection 2.6. Although we aim to provide the complete code snippets for each test case, some lines that are not essential to understanding the examples are omitted for brevity. The omitted scripts are provided in the appendix, and readers are referred to the original source code for the complete implementations.

4.1. Reporting the numerical results from the Lorenz 63 model.

We briefly dedicate this part to the discussion of the results – presented in Fig. 12 – obtained when executing the script in Listing 11. Here, we compare the performance of the four DA methods in the estimation of the first parameter and first state variable (x_1 and x_4 respectively), as well as the comparison in the observation space. The true values are shown alongside the DA predictions, with a confidence interval of 2σ for the EnKF and UKF (visible only in the first plot, whereas the interval collapses in the remaining ones), since these two propagate a `SecondMoment` throughout the loop; on the other hand, the SIR and variational methods do not propagate any uncertainty, and therefore no confidence interval is shown. The EnKF and UKF are able to accurately estimate the true unknowns, both in the augmented state space and in the observation space. The same is true for the variational method, although about 4 assimilation windows are needed for the estimates to converge to the true values for x_4 and the observations, and longer still for x_1. Another downside of the latter method is that its simulations have cost us $\sim \mathcal{O}(10^3)$ more in time than the Bayesian filters, even with the automatic differentiation capabilities we exploit from SciMLSensitivity. On the other hand, the SIR is unable to accurately estimate all three unknowns, as its predictions diverge from the true values after a few time steps. We believe that SIR, and more generally our `ParticleFilters`, are less

bias_aware_oscillator.jl

```julia
# True transition model
true_μ = Realisation([[55.0,75.0,3.4]])
true_probl = ODEWrapper(
  Tsit5(),oscillator!,u0,ts[ALL],true_μ
)
true_transition = Model(true_probl)
true_history = execute(true_transition,ts)

# Transition model with warmup
nparams = 10
μ = realisation(pspace;nparams)
u0μ = ParamArray(u0[1],nparams)
probl = ODEWrapper(Tsit5(),oscillator!,u0μ,ts[ALL],μ)
transition = MemoryModel(probl)
history = execute(transition,ts,WARMUP)

# Observation model
N_p = dimension(pspace)
N_u = dimension(u0)
N_obs = 1
observation = build_linear_observation_model(
  1:(N_p+N_u),[N_p+1]
)

# Synthetic observations from true history
σ_obs = 0.1
obs_noise = Noise(σ_obs^2 * I(N_obs))
da_true_states = collect_forecasted_states(
  true_history[OBSDA]
)
obs´ = build_observations(
  observation,da_true_states,obs_noise,bias
)
obs = expand(obs´,ts[OBSDA],ts[DA])

# Compute esn, i.e. the trained bias model

# Initialise prior distribution
nensemble = 30
μ = realisation(pspace;nparams=nensemble)
u0μ = ParamArray(u0[1],nensemble)
probl = ODEWrapper(Tsit5(),oscillator!,u0μ,ts[ALL],μ)
transition = MemoryModel(probl)
history = execute(transition,ts,WARMUP)

seed_state = collect_forecasted_state(
  history[OBSWARMUP]
)
init_cov_p = Noise(diagm([0.5,0.5,0.05].^2))
init_cov_u = Noise(diagm([1e-2,1e-2].^2))
init_cov = joint_law(init_cov_p,init_cov_u)
constraints = BlockConstraint(
  ConstrainTo(pspace),NoConstraint()
)
prior = build_prior(
  seed_state,init_cov,constraints;nsamples=nensemble
)

# DA
inflation = MultInflation(1.005)
ienkf = InflationKalmanFilter(
  transition,observation,prior;
  obs_noise,inflation
)
bienkf = BiasAwareKalmanFilter(
  ienkf,esn,obs_noise;γ=0.001
)

results = loop(bienkf,obs)
```

FIGURE 13. Code snippet used to run the DA for the Van der Pol example.

effective than the KF variants in parameter-state estimation problems, and they perform better in state-only estimation problems – as demonstrated by the flat estimate of x_1. In addition, the application of SIR here is less natural than the remaining DA methods, since the Gaussian assumption holds here.
The better performance of EnKF and UKF, as well as the nature of our numerical tests, motivate our choice of using the EnKF as the main DA strategy we employ in the next subsections.

4.2. **Bias-aware EnKF on the Van der Pol oscillator.** In this example, we consider a bias-aware EnKF procedure for the state-parameter estimation of a Van der Pol oscillator [58] with biased observations. This numerical test is inspired by [23], which employs the same approach to a similar benchmark. The transition and observation models are given by:

$$\boldsymbol{\mathcal{F}}(\boldsymbol{x}) \doteq \begin{bmatrix} x_5 \\ -\omega^2 x_4 + x_5(x_2 - x_1) - x_5 \frac{x_3 x_4^2}{1+(x_3/x_2)x_4^2} \end{bmatrix}, \qquad \boldsymbol{\mathcal{H}}(\boldsymbol{x}) \doteq x_4 + \cos(x_4), \qquad \boldsymbol{x} = \begin{bmatrix} \boldsymbol{\mu} \\ \hline \boldsymbol{u} \end{bmatrix} \doteq \begin{bmatrix} x_1 \\ x_2 \\ x_3 \\ \hline x_4 \\ x_5 \end{bmatrix}$$

where $\omega \doteq 240\pi$. The first three entries of $\boldsymbol{x}$ correspond to the parameters $\boldsymbol{\mu} \equiv (x_1, x_2, x_3)^T \in \mathbb{R}^3$, while the last two entries correspond to the state $\boldsymbol{u} \equiv (x_4, x_5)^T \in \mathbb{R}^2$. The sensors record the first state variable corrupted by a cosine bias term, that is $\boldsymbol{b}(\boldsymbol{x}) \doteq \cos(x_4)$. Observations are recorded once every 5 time steps. After an initial spin-up phase, the bias model is trained on synthetic data obtained by running the transition operator on an ensemble of initial conditions. This strategy is widely adopted in the RC community, as it allows the ESN modelling the bias to be trained so that it is largely independent of the initial conditions, thus achieving better generalisation capabilities. The training is performed using the recycle validation strategy proposed in [23, 41]. Following the training is the washout – another technique frequently encountered in the context of ESNs – whose primary purpose is to correctly initialise the network once the training is complete [43].

The code for this test is reported in two separate figures: in Listing 13 we show the main code snippet, whereas in Listing 14 we show the code for the training of the bias model. The missing code – primarily used to set up the problem – is reported

train_bias_model.jl

```julia
# Bias
bias(x) = [cos(x[N_p+1])]

# Bias-model training data
true_train_states = collect_forecasted_states(
  true_history[OBSTRAIN]
)
train_states = collect_forecasted_means(
  history[OBSTRAIN]
)
true_train_obs = build_observations(
  observation,true_train_states,bias
)
pred_train_obs = build_observations(
  observation,true_train_states
)
true_bias_train = true_train_obs - pred_train_obs
@views train_data = true_bias_train[:,1:end-1]
@views target_data = true_bias_train[:,2:end]

# Bias model
N_r = 100
χ = maximum(abs,train_data)
rng = MersenneTwister(1234)
esn = NovoaEchoStateNetwork(
  N_obs,N_r,N_obs;
  rng=rng,connect=5,
  modifier_in=Modifier(
    Normalisation(fill(χ,N_obs)),AddBias(0.1)
  ),
  modifier_state=Modifier(AddBias(1.0)),
  activation=tanh
)

# Train bias model (recycle validation)
Ngrid = 60
radius = 0.5:(1.05-0.5)/(Ngrid-1):1.05
scaling = 0.05:(3.0-0.05)/(Ngrid-1):3.0
tikhonov = (1e-16,1e-12,1e-8)

method = TrainRecurrentNeuralNetwork(;
  augmentation=DataAugmentation((-0.1,0.01)),
  regularisation=DataRegularisation(train_data),
  λ=1e-8,forget=30
)

rvmethod = RecycleValidation(
  method,tikhonov,radius,scaling;
  Nfolds=15,Ntrain=size(train_data,2),Nvalidation=200
)
_ = train(rvmethod,esn,train_data,target_data)

# Washout
true_wash_states = collect_forecasted_states(
  true_history[OBSWASHOUT]
)
true_spread_states = collect_forecasted_states(
  true_history[OBSSPREAD]
)
true_wash_obs = build_observations(
  observation,true_wash_states,bias
)
true_spread_obs = build_observations(
  observation,true_spread_states,bias
)
pred_wash_obs = build_observations(
  observation,true_wash_states
)
pred_spread_obs = build_observations(
  observation,true_spread_states
)
wash_spread_data = hcat(
  true_wash_obs-pred_wash_obs,
  true_spread_obs-pred_spread_obs
)
reset_state!(esn)
_ = esn(wash_spread_data)
```

FIGURE 14. Code snippet used to define and train the bias model for the Van der Pol example.

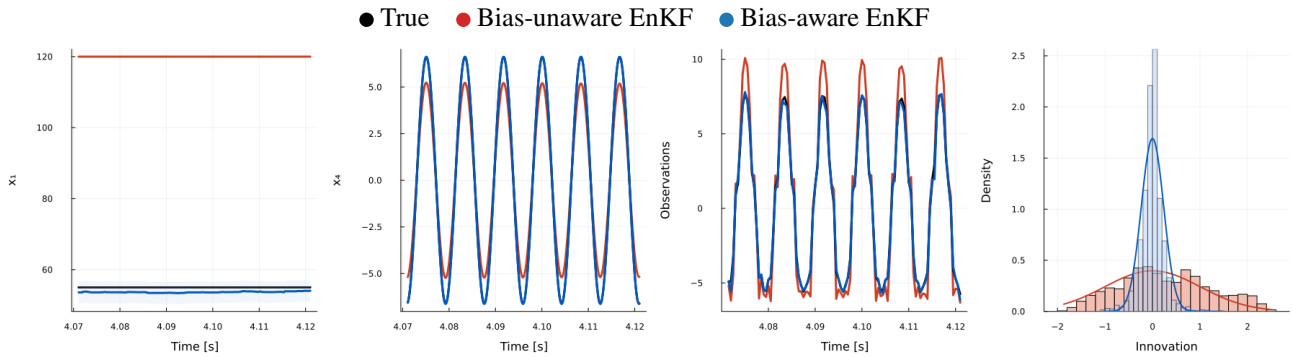

FIGURE 15. Van der Pol example. From left to right: (i) estimation of $x_1 \equiv \mu_1$ in the last $0.5s$ of the assimilation window, (ii) estimation of $x_4 \equiv u_1$ in the last $0.5s$ of the assimilation window, (iii) estimation of observations in the last $0.5s$ of the assimilation window, and (iv) estimated probability density function of the innovation.

in Appendix A. The main novelties presented in the snippets shown here with respect to those discussed in the previous section are:

- Lines $31-34$ of Listing 13: an additional bias function can be supplied to the `build_observations` method (previously discussed in Subsection 3.5) to generate biased observations.
- Lines $59-69$ of Listing 13: a bias-aware EnKF filter with fixed multiplicative inflation $\rho \doteq 1.005$ is defined, and the DA is performed with a regularisation parameter $\gamma \doteq 10^{-3}$ (see Eq. (8)).

navier_stokes.jl

```julia
# True transition model
true_μ = realisation(ptspace,sampling=:uniform)
true_ic = initial_condition(true_μ)
true_fesol = solve(ode_solver,feop,true_μ,true_ic)
true_transition = TransientPDEModel(true_fesol)

# Transition model with warmup
nparams = 30
μ = realisation(ptspace;nparams)
ic = initial_condition(μ)
fesol = solve(ode_solver,feop,μ,ic)
transition = MemoryModel(fesol)
warmup!(transition,ts)

# Observation model
step = 2
N_p = dimension(pspace)
N_u = dimension(Y)
M = N_p+N_u
N_obs = Int(M/step)
observation = build_linear_observation_model(
  1:M,(N_p+1):step:M
)

# Synthetic observations from true history
σ_obs = 0.5
obs_noise = Noise(σ_obs^2 * I(N_obs))
true_history = execute(true_transition,ts)
da_true_states = collect_forecasted_states(
  true_history[OBSDA]
)
obs´ = build_observations(
  observation,da_true_states,obs_noise
)
obs = expand(obs´,ts[OBSDA],ts[DA])

# DA
prior = copy(transition.prior)
enkf = EnsembleKalmanFilter(
  transition,observation,prior;obs_noise
)
results = loop(enkf,obs)
```

FIGURE 16. Code snippet used to run the DA for the Navier-Stokes example.

- Lines $18-19$ of Listing 14: the training data used to train the ESN is constructed so that the network is taught to predict, at any given time step, the cosine bias term of the observations at the next time step. This explains why `target_data` is defined by shifting `train_data` by a single time step.
- Lines $21-33$ of Listing 14: an ESN with $N_r \doteq 100$ hidden units is defined, with a $\tanh$ activation function and a bias term added to the input (which is normalised) and state. The keyword `connect` is related to the number of nonzero entries of the sparse reservoir matrix, while `rng` is used to seed the random number generator for reproducibility.
- Lines $35-51$ of Listing 14: the ESN is trained with the recycle validation strategy proposed in [23, 41], which is a cross-validation technique that allows the best hyperparameters of the network to be selected. The training data is augmented and regularised by means of additive Gaussian noise, which was shown in [41] to yield more accurate forecasting by the network. Following the example of [23], the hyperparameters consist of the spectral radius, the input scaling, and the Tikhonov regularisation parameter. The best hyperparameters are then used to train the final model.
- Lines $53-77$ of Listing 14: the washout phase is run to correctly initialise the ESN before employing it in the DA window.

The performance of the bias-aware EnKF, along with a comparison with a bias-unaware counterpart (simply given by the inflation EnKF defined at lines $61-64$ of Listing 13), is shown in Figure 15. The first two plots compare the predicted values of x_1 and x_4, respectively, and show how the bias-unaware option is unable to recover the true solution. This is expected, since the biased observations will never allow the filter to converge to a zero-mean Gaussian distribution for the innovation (as demonstrated by the fourth plot), which is a fundamental assumption of KFs. On the other hand, the bias-aware model recovers accurate estimates both in the parameter-state space (first two plots) and in the observation space (third plot). In particular, the predicted values of x_4 and the observations perfectly overlap with the true values. The fourth plot shows that the bias-aware filter accurately recovers the Gaussian assumption probability density function (PDF) for the innovation.

4.3. **Discovering the Reynolds number of a turbulent Navier-Stokes flow.** In this example, we consider an EnKF procedure for the parameter-state estimation of an incompressible turbulent Navier-Stokes flow around a square cavity in a 2D rectangular domain. We consider homogeneous no-slip conditions on the top and bottom walls, a constant inflow profile on the inlet (left wall), a no-penetration condition on the outlet (right wall), and an initial condition obtained from the solution of a (steady-state) Stokes equation at $t = 0$. We add a SUPG stabilisation term to the momentum equation, whose weak formulation therefore reads as:

$$\int_\Omega \frac{d\boldsymbol{u}}{dt}\boldsymbol{v} + \int_\Omega (\boldsymbol{u}\cdot\nabla)\boldsymbol{u}\boldsymbol{v} + \int_\Omega \nu\nabla\boldsymbol{u} : \nabla\boldsymbol{v} - \int_\Omega p(\nabla\cdot\boldsymbol{v}) + \int_\Omega (\nabla\cdot\boldsymbol{u})q + \int_\Omega \tau(\boldsymbol{u}\cdot\nabla)\boldsymbol{v}\cdot\boldsymbol{r}, \tag{16}$$
$$\boldsymbol{r} = \frac{d\boldsymbol{u}}{dt} + \nabla\cdot(\nu\nabla\boldsymbol{u}) + (\boldsymbol{u}\cdot\nabla)\boldsymbol{u} - \nabla p.$$

The SUPG stabilisation term is given by the last integral in (16), where τ is a stabilisation parameter that depends on the local mesh size and the flow velocity [59]. The parameters of the considered problem are the viscosity and the inflow velocity in the horizontal direction, i.e. $\boldsymbol{\mu} \equiv (u_{\text{in}}, \nu)^T \in \mathbb{R}^2$. We consider a parameter space $(0.1, 0.4) \times (10^{-6}, 10^{-5})$,

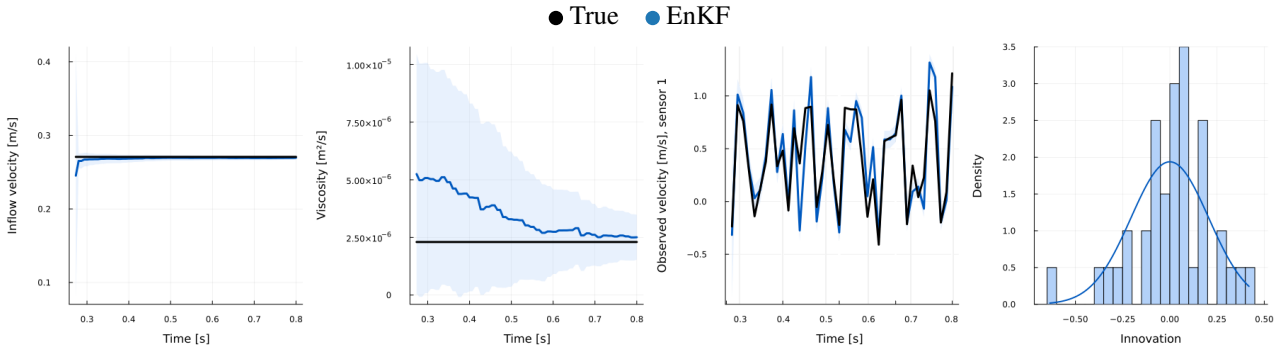

FIGURE 17. Navier-Stokes example. From left to right: (i) estimation of $x_1 \equiv u_{\text{in}}$ in the last $0.5s$ of the assimilation window, (ii) estimation of $x_2 \equiv \nu$ in the last $0.5s$ of the assimilation window, (iii) estimation of observations in the last $0.5s$ of the assimilation window, and (iv) estimated probability density function of the innovation.

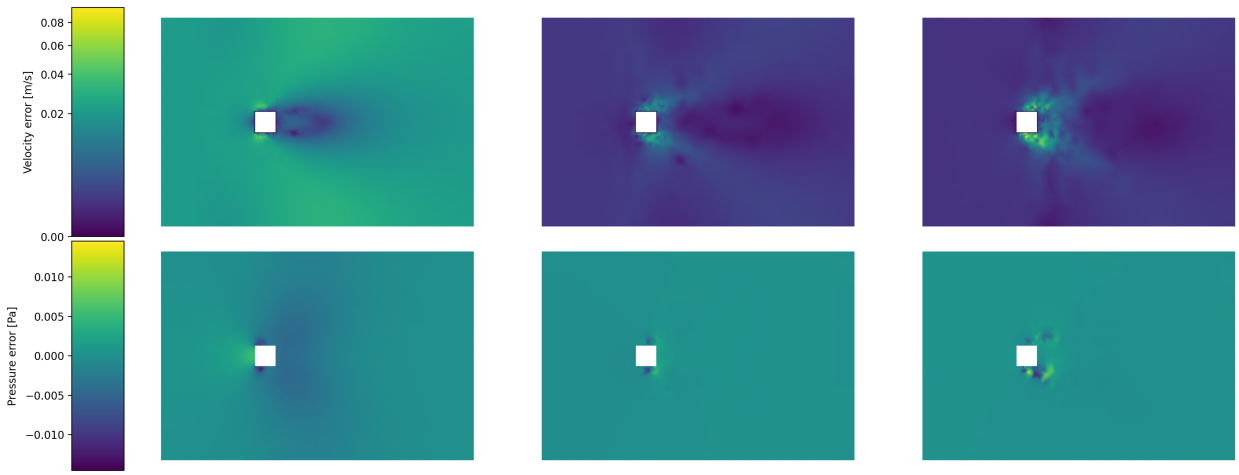

FIGURE 18. Velocity (top) and pressure (bottom) errors for the Navier-Stokes test at three time steps. From left to right: $t \doteq t^{20}$, $t \doteq t^{40}$, and $t \doteq t^{60}$.

and since the characteristic length of the domain is $L = 0.04$, the Reynolds number lies in the range $(400, 16000)$. A P2-P1 pair of Taylor-Hood FEs is employed for the spatial discretisation, whereas a generalised α-method is used for the time marching. At every time step, a Newton-Raphson method is used to solve the linearised system. We refer to Appendix B for the script used to set up the experiment for additional details. This benchmark is run using a standard EnKF over $N_t \doteq 80$ DA time steps, after executing 40 warmup iterations. A sensor records every other state variable (velocities and pressures only), and observation measurements occur every other time step, as shown in Figure 1.

Though this application is simpler than the previous one from a purely DA perspective, it still remains challenging due to its highly nonlinear nature. Even a slight deviation from the true parameters or states may lead the Newton solver to diverge, and thus the entire filter. For this reason, we remark that too big a departure of the initial ensemble from the true values may result in filter divergence, and thus must be chosen with care. As shown in Figs. 17-18, the EnKF is able to overcome these challenges and accurately recover the true values of the parameters, states and observations. Notably, the fourth plot shows that the innovation is accurately modelled by a zero-mean Gaussian distribution, which confirms that the assumptions of the EnKF are satisfied. The results demonstrate the aptness of our framework in estimating the hidden Reynolds number of a turbulent flow. Though the dimension of the state (~ 6500 degrees of freedom (DOFs)) is not intractable, the computational cost of this problem remains high, and the use of a model surrogate, though advisable, is not straightforward due to the highly nonlinear nature of the problem.

4.4. **Data assimilation with model surrogate for the Heat equation.** In this example, we consider an EnKF procedure for the parameter-state estimation of a Heat equation on a unit square. A comparison is made between DA loops obtained with transition operators given by (i) the FE method, (ii) a reduced basis (RB) surrogate, and (iii) a RB surrogate with the kriging calibration described in Subsection 2.6. We consider non-homogeneous Dirichlet boundary conditions on the left wall, non-homogeneous Neumann boundary conditions on the right wall, and homogeneous Neumann boundary conditions

rom_kriging_calibration.jl

```julia
# True transition model
true_μ = realisation(ptspace,sampling=:uniform)
true_fesol = solve(solver,feop,true_μ,uh0μ)
true_transition = TransientPDEModel(true_fesol)

# Transition model with warmup
nparams = 30
μ = realisation(ptspace;nparams)
fesol = solve(solver,feop,μ,uh0μ)
transition = MemoryModel(fesol)
warmup!(transition,ts)

# Observation model
step = 10
N_p = dimension(pspace)
N_u = dimension(V)
M = N_p+N_u
N_obs = Int(M/step)
observation = build_linear_observation_model(
  1:M,(N_p+1):step:M
)

# Synthetic observations from true history
σ_obs = 0.5
obs_noise = Noise(σ_obs^2 * I(N_obs))
true_history = execute(true_transition,ts)
da_true_states = collect_forecasted_states(
  true_history[OBSDA]
)
obs´ = build_observations(
  observation,da_true_states,obs_noise
)
obs = expand(obs´,ts[OBSDA],ts[DA])

# DA - FEM
prior = copy(transition.prior)
enkf = KalmanFilter(
  transition,observation,prior;obs_noise
)
results_fem = loop(enkf,obs)

# DA -ROM
tol = 1e-4
nparams_off = 80
μ_off = realisation(ptspace;nparams=nparams_off)
state_reduction = SteadyReduction(
  tol,H1();nparams=nparams_off,sketch=:sprn,
  hypred_strategy=:rbf
)
rbsolver = RBSolver(solver,state_reduction)
fesnaps, = solution_snapshots(rbsolver,feop,μ_off,uh0μ)
rbop = reduced_operator(rbsolver,feop,fesnaps)

rbsol = solve(solver,rbop,μ,uh0μ)
rbtransition = MemoryModel(rbsol)
warmup!(rbtransition,ts)

rbprior = copy(rbtransition.prior)
rbenkf = KalmanFilter(
  rbtransition,observation,rbprior;obs_noise
)

# DA - Calibrated ROM
nparams_start = 30
μ_cal = μ_off[(nparams_start+1):nparams_off,:]
rbsnaps, = solution_snapshots(rbsolver,rbop,μ_cal,uh0μ)
calibration = KrigingCalibration(
  observation,fesnaps,rbsnaps,ts
)
crbenkf = CalibratedKalmanFilter(rbenkf,calibration)
results_krig = loop(crbenkf,obs)
```

FIGURE 19. Code snippet used to run the DA for the Heat equation example.

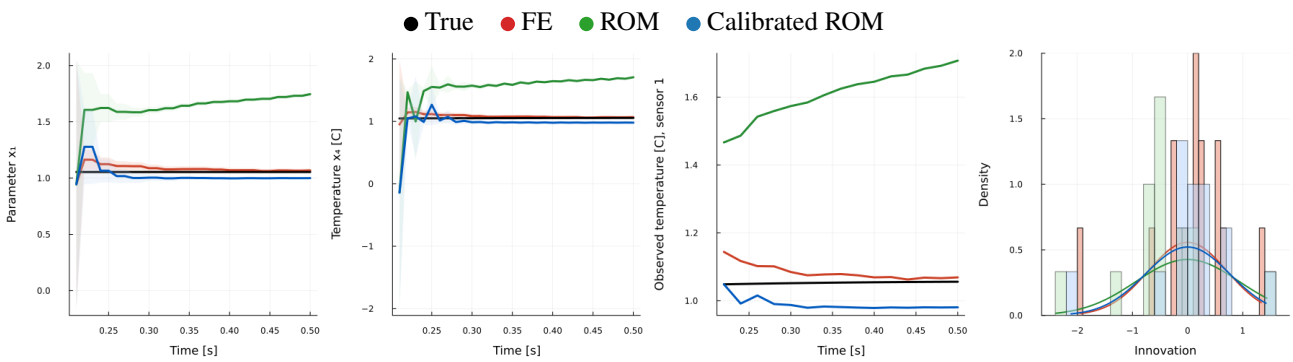

FIGURE 20. Heat equation example. From left to right: (i) estimation of $x_1 \equiv \mu_1$ in the last $0.5s$ of the assimilation window, (ii) estimation of $x_4 \equiv u_1$ in the last $0.5s$ of the assimilation window, (iii) estimation of observations in the last $0.5s$ of the assimilation window, and (iv) estimated probability density function of the innovation.

on top and bottom walls. The problem's weak formulation reads as:

$$\int_\Omega \frac{du}{dt} v + \int_\Omega \alpha \nabla u \cdot \nabla v = \int_\Omega v, \qquad u = u_{\mathrm{D}} \quad \text{on} \quad \{0\} \times (0,1), \qquad -\alpha \nabla u \cdot \boldsymbol{n} = u_{\mathrm{N}} \quad \text{on} \quad \{1\} \times (0,1),$$

where

$$\alpha(\boldsymbol{x}; t, \boldsymbol{\mu}) = 1 + \exp\left(-\sin(t)^2 \, x_1 / \sum_i \mu_i\right), \qquad u_{\mathrm{D}}(\boldsymbol{x}; t, \boldsymbol{\mu}) = \mu_1 \exp\left(-x_2/\mu_3\right), \qquad u_{\mathrm{N}}(\boldsymbol{x}; t, \boldsymbol{\mu}) = \left|\cos\left(t/\mu_2\right)\right|.$$

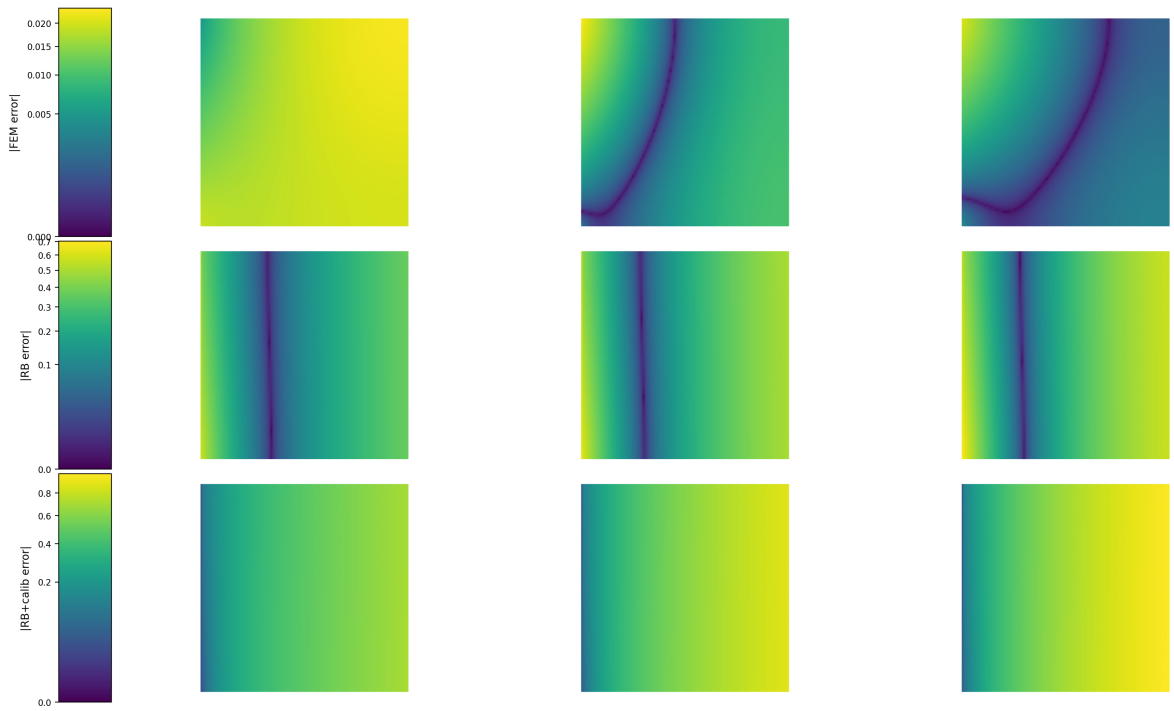

FIGURE 21. Heat equation errors at three time steps. From left to right: $t \doteq t^{10}$, $t \doteq t^{20}$, and $t \doteq t^{30}$.

The parameters of the considered problem are $\boldsymbol{\mu} \equiv (\mu_1, \mu_2, \mu_3)^T \in \mathbb{R}^3$, which are constrained to lie in the parametric domain $(1, 10)^3$. A P1 FE is employed for the spatial discretisation, whereas a Backward Euler integrator is used for time integration. The problem is initialised from a homogeneous initial condition at $t = 0$. Observations are recorded at every other time step, and one sensor is placed at every 10 spatial DOFs. The core of the parameter-estimation procedure is illustrated in Listing 19, whereas the missing lines of code are reported in the Appendix C. This experiment is run using a standard EnKF over $N_t \doteq 30$ DA time steps, after executing 20 warmup iterations.

The results of the DA procedure are shown in Figs. 20-21. From Fig. 20, it appears that the calibrated ROM greatly outperforms the standard ROM in terms of accuracy. Indeed, the latter seems to not converge to the right values, due to the relatively high ROM errors with respect to the observation errors, which cause the analysis step to correct to a wrong value. However, Fig. 21 depicts a more unclear picture, as it shows the calibrated filter does not uniformly outperform the standard ROM in terms of accuracy in all state variables. From this, it appears that the second plot of Fig. 20 demonstrating how well the calibrated ROM estimates x_4 compared to the plain ROM is possibly a "lucky" shot. Indeed, x_4 is the temperature value recorded at the point $(0.01, 0)$, which appears to be in a region of the domain where the calibrated ROM error is relatively low. Interestingly, the same is true for the parameters: though we empirically verified that parameters are generally better captured by the calibrated ROM, we have also simulated scenarios where some parameters are better estimated by the standard ROM. This is not incompatible with the findings of [22], which show that the kriging calibration is able to reduce the ROM error in the observation space, but not necessarily in the parameter-state space. A better option to improve the accuracy of the ROM surrogate would have been, in this instance, to increase the accuracy of the ROM itself by increasing the number of RB basis functions, rather than relying on the kriging calibration. These findings are a motivation to explore alternative ROM error-aware methods in future work. In any case, Listing 19 demonstrates how easy it is to implement DA loop with surrogate models, both calibrated and standard. Lastly, we remark that the ROM surrogate is about 15 times cheaper than the FE model in memory (13.56 Gb for the FE, 0.91 Gb for the ROM), whereas the calibrated ROM is ≈ 2.7 times cheaper; these significant speed-up measures demonstrate the usefulness of ROM surrogates in DA frameworks.

5. CONCLUSIONS

In this work, we introduce Opals, a Julia package that provides a unified framework for sequential and variational inference for a variety of dynamical systems. The package is designed to be composable, allowing users to build complex inference tools by combining basic methods with advanced capabilities. Opals integrates natively with the SciML ecosystem for ODE-governed systems and with Gridap/GridapROMs for both full-order and reduced-order discretisations of PDEs. We demonstrate the library on several examples, including a Lorenz-63 benchmark, a Van der Pol oscillator problem with biased observations, a turbulent Navier-Stokes flow past a square cavity, and a heat equation using a model surrogate. The results show that Opals can effectively estimate hidden states and uncertain parameters from partial, noisy, and potentially biased observational data. These numerical experiments are challenging, as they combine a wide range of concepts and implementation building blocks, such as ROMs, strongly nonlinear saddle-point dynamics, and RC-based correction of

structural model errors.

We envision three main directions for future work. First, we plan to include multi-fidelity inference methods, which can leverage the availability of multiple models of varying fidelity to improve accuracy for a given computational budget. A first step in this direction could be to insert our existing ROM frameworks within the multi-fidelity pipelines, although we may eventually develop more advanced strategies, such as recently emerging deep learning approaches [60]. Second, we plan to develop a more comprehensive suite of ROMs for PDE-governed systems, and to further strengthen the ROM error-aware strategies available in the library. Finally, we plan to extend the library to handle more complex applications, mainly in the context of hydrodynamics and fluid-structure interaction problems, which are of particular interest to us within the scope of offshore engineering.

Acknowledgments

This publication is part of the DigiOcean4Solar project, with file number 21225, of the NWO Talent Programme Vidi AES 2023, which is financed by the Dutch Research Council (NWO) under grant ID 10.61686/OPCTU16570.

References

[1] R. Daley, Atmospheric Data Analysis, Cambridge Atmospheric and Space Science Series, Cambridge University Press, 1991.
[2] A. F. Bennett, Inverse Modeling of the Ocean and Atmosphere, Cambridge University Press, 2002.
[3] C. Wunsch, The Ocean Circulation Inverse Problem, Cambridge University Press, 1996.
[4] C. D. Rodgers, Inverse Methods for Atmospheric Sounding: Theory and Practice, World Scientific, 2000.
[5] M. P. Anderson, W. W. Woessner, R. J. Hunt, Applied Groundwater Modeling: Simulation of Flow and Advective Transport, 2nd Edition, Academic Press, 2015.
[6] W. Menke, Geophysical Data Analysis: Discrete Inverse Theory, 4th Edition, Academic Press, 2018.
[7] A. Manzoni, S. Pagani, T. Lassila, Accurate solution of bayesian inverse uncertainty quantification problems combining reduced basis methods and reduction error models, SIAM/ASA Journal on Uncertainty Quantification 4 (1) (2016) 380–412. doi:10.1137/15M1021948.
[8] R. E. Kalman, A new approach to linear filtering and prediction problems, Journal of Basic Engineering 82 (1) (1960) 35–45. doi:10.1115/1.3662552.
[9] A. Doucet, N. de Freitas, N. Gordon (Eds.), Sequential Monte Carlo Methods in Practice, Springer, New York, 2001. doi:10.1007/978-1-4757-3437-9.
[10] A. C. Lorenc, Analysis methods for numerical weather prediction, Quarterly Journal of the Royal Meteorological Society 112 (474) (1986) 1177–1194. doi:10.1002/qj.49711247414.
[11] O. Talagrand, P. Courtier, Variational assimilation of meteorological observations with the adjoint vorticity equation. i: Theory, Quarterly Journal of the Royal Meteorological Society 113 (478) (1987) 1311–1328. doi:10.1002/qj.49711347812.
[12] O. R. A. Dunbar, I. Lopez-Gomez, A. G.-I. nigo, D. Z. Huang, E. Bach, J. long Wu, Ensemblekalmanprocesses.jl: Derivative-free ensemble-based model calibration, Journal of Open Source Software 7 (80) (2022) 4869. doi:10.21105/joss.04869.
[13] F. B. Carlson, Lowlevelparticlefilters.jl, https://github.com/baggepinnen/LowLevelParticleFilters.jl, gitHub repository, accessed 2026.
[14] H. Ge, K. Xu, Z. Ghahramani, Turing: A language for flexible probabilistic inference, Proceedings of the Twenty-First International Conference on Artificial Intelligence and Statistics (AISTATS) 84 (2018) 1682–1690.
[15] M. F. Cusumano-Towner, F. A. Saad, A. K. Lew, V. K. Mansinghka, Gen: A general-purpose probabilistic programming system with programmable inference, in: Proceedings of the 40th ACM SIGPLAN Conference on Programming Language Design and Implementation (PLDI), 2019, pp. 221–236. doi:10.1145/3314221.3314642.
[16] C. Rackauckas, Y. Ma, J. Martensen, C. Warner, K. Zubov, R. Supekar, D. Skinner, A. Ramadhan, A. Edelman, Universal differential equations for scientific machine learning (2021). arXiv:2001.04385.
URL https://arxiv.org/abs/2001.04385
[17] J. Behrensdorf, A. Gray, A. Perin, J. Grashorn, M. Luttmann, L. Fritsch, F. Belik, M. Broggi, F. Mett, M. Bittner, L. Knipper, M. Behrendt, M. Schmidt, Uncertaintyquantification.jl (Jul. 2026). doi:10.5281/zenodo.21628961.
URL https://doi.org/10.5281/zenodo.21628961
[18] V. Dixit, C. Rackauckas, Globalsensitivity.jl: Performant and parallel global sensitivity analysis with julia, Journal of Open Source Software 7 (76) (2022) 4561. doi:10.21105/joss.04561.
[19] T. M. Hamill, J. S. Whitaker, Distance-dependent filtering of background error covariance estimates in an ensemble kalman filter, Monthly Weather Review 129 (11) (2001) 2776–2790. doi:10.1175/1520-0493(2001)129<2776:DDFOBE>2.0.CO;2.

[20] H.-X. Sun, S. Wang, X. Zheng, S. X. Chen, High-dimensional ensemble kalman filter with localization, inflation, and iterative updates, Quarterly Journal of the Royal Meteorological Society 150 (765) (2024) 4870–4884. doi:10.1002/qj.4846.
[21] T. Berry, T. Sauer, Adaptive ensemble kalman filtering of non-linear systems, Tellus A: Dynamic Meteorology and Oceanography 65 (1) (2013) 20331. doi:10.3402/tellusa.v65i0.20331.
[22] S. Pagani, A. Manzoni, A. Quarteroni, Efficient state/parameter estimation in nonlinear unsteady pdes by a reduced basis ensemble kalman filter, SIAM/ASA Journal on Uncertainty Quantification 5 (1) (2017) 890–921. doi:10.1137/16M1078598.
[23] A. Nóvoa, A. Racca, L. Magri, Inferring unknown unknowns: Regularised bias-aware ensemble kalman filter, Computer Methods in Applied Mechanics and Engineering 418 (2024) 116502. doi:10.1016/j.cma.2023.116502.
[24] S. Badia, F. Verdugo, Gridap: An extensible Finite Element toolbox in Julia, Journal of Open Source Software 5 (52) (2020) 2520. doi:10.21105/joss.02520.
URL https://doi.org/10.21105/joss.02520
[25] N. Mueller, S. Badia, Gridaproms.jl: Efficient reduced order modelling in the julia programming language (2025). arXiv:2503.15994.
URL https://arxiv.org/abs/2503.15994
[26] P.-B. Rubio, L. Chamoin, F. Louf, Real-time bayesian data assimilation with data selection, correction of model bias, and on-the-fly uncertainty propagation, Comptes Rendus Mécanique 347 (11) (2019) 762–779. doi:10.1016/j.crme.2019.11.004.
[27] A. F. C. da Silva, T. Colonius, Flow state estimation in the presence of discretization errors, Journal of Fluid Mechanics 890 (2020) A10. doi:10.1017/jfm.2020.103.
[28] F. Chinesta, E. Cueto, E. Abisset-Chavanne, J. L. Duval, F. E. Khaldi, Virtual, digital and hybrid twins: A new paradigm in data-based engineering and engineered data, Archives of Computational Methods in Engineering 27 (1) (2020) 105–134. doi:10.1007/s11831-018-9301-4.
[29] M. Bonavita, P. Laloyaux, Machine learning for model error inference and correction, Journal of Advances in Modeling Earth Systems 12 (12) (2020) e2020MS002232. doi:10.1029/2020MS002232.
[30] S. E. Cohn, D. P. Dee, Observability of discretized partial differential equations, SIAM Journal on Numerical Analysis 25 (3) (1988) 586–617. doi:10.1137/0725037.
[31] G. H. Golub, C. F. V. Loan, Matrix Computations, 4th Edition, Johns Hopkins University Press, Baltimore, MD, 2013.
[32] A. H. Jazwinski, Stochastic Processes and Filtering Theory, Vol. 64 of Mathematics in Science and Engineering, Academic Press, New York, 1970.
[33] T. Berry, T. Sauer, Adaptive ensemble kalman filtering of nonlinear systems, Tellus A: Dynamic Meteorology and Oceanography 65 (2013) 20331. doi:10.3402/tellusa.v65i0.20331.
[34] P. Sakov, P. R. Oke, A deterministic formulation of the ensemble kalman filter: An alternative to ensemble square root filters, Tellus A: Dynamic Meteorology and Oceanography 60 (2) (2008) 361–371. doi:10.1111/j.1600-0870.2007.00299.x.
[35] G. Evensen, et al., Data assimilation: the ensemble Kalman filter, Vol. 2, Springer, 2009.
[36] G. Burgers, P. J. van Leeuwen, G. Evensen, Analysis scheme in the ensemble kalman filter, Monthly Weather Review 126 (6) (1998) 1719–1724. doi:10.1175/1520-0493(1998)126<1719:ASITEK>2.0.CO;2.
[37] J. L. Anderson, Spatially and temporally varying adaptive covariance inflation for ensemble filters, Tellus A: Dynamic Meteorology and Oceanography 61 (1) (2009) 72–83. doi:10.1111/j.1600-0870.2008.00361.x.
[38] C. H. Bishop, J. S. Whitaker, L. Lei, Gain form of the ensemble transform kalman filter and its relevance to satellite data assimilation with model space ensemble covariance localization, Monthly Weather Review 145 (11) (2017) 4575–4592. doi:10.1175/MWR-D-17-0102.1.
[39] G. Gaspari, S. E. Cohn, Construction of correlation functions in two and three dimensions, Quarterly Journal of the Royal Meteorological Society 125 (554) (1999) 723–757. doi:10.1002/qj.49712555417.
[40] R. Mehra, On the identification of variances and adaptive kalman filtering, IEEE Transactions on Automatic Control 15 (2) (1970) 175–184. doi:10.1109/TAC.1970.1099422.
[41] A. Nóvoa, L. Magri, Real-time thermoacoustic data assimilation, Journal of Fluid Mechanics 948 (2022) A35. doi:10.1017/jfm.2022.653.
[42] H. Jaeger, The "echo state" approach to analysing and training recurrent neural networks, Tech. Rep. 148, German National Research Center for Information Technology (GMD), Sankt Augustin, Germany (2001). doi:10.24406/publica-fhg-291111.
[43] M. Lukoševičius, A practical guide to applying echo state networks, in: G. Montavon, G. B. Orr, K.-R. Müller (Eds.), Neural Networks: Tricks of the Trade, 2nd Edition, Vol. 7700 of Lecture Notes in Computer Science, Springer, Berlin, Heidelberg, 2012, pp. 659–686. doi:10.1007/978-3-642-35289-8_36.
[44] A. Quarteroni, G. Rozza, Reduced Order Methods for Modeling and Computational Reduction, 2014. doi:10.1007/978-3-319-02090-7.
[45] F. Negri, A. Manzoni, G. Rozza, Reduced basis approximation of parametrised optimal flow control problems for the Stokes equations, Computers & Mathematics with Applications 69 (4) (2015) 319–336.

[46] R. Tenderini, N. Mueller, S. Deparis, Space-time reduced basis methods for parametrised unsteady stokes equations, SIAM Journal on Scientific Computing 46 (1) (2024) B1–B32. arXiv:https://doi.org/10.1137/22M1509114, doi:10.1137/22M1509114.
URL https://doi.org/10.1137/22M1509114

[47] N. Mueller, S. Badia, Model order reduction with novel discrete empirical interpolation methods in space–time, Journal of Computational and Applied Mathematics 444 (2024) 115767. doi:https://doi.org/10.1016/j.cam.2024.115767.
URL https://www.sciencedirect.com/science/article/pii/S0377042724000165

[48] N. Mueller, Y. Zhao, S. Badia, T. Cui, A tensor-train reduced basis solver for parameterised partial differential equations on cartesian grids, Journal of Computational and Applied Mathematics 472 (2026) 116790. doi:https://doi.org/10.1016/j.cam.2025.116790.
URL https://www.sciencedirect.com/science/article/pii/S0377042725003048

[49] J.-P. Chilès, P. Delfiner, Geostatistics: Modeling Spatial Uncertainty, Wiley Series in Probability and Statistics, John Wiley & Sons, New York, 1999.

[50] S. J. Julier, J. K. Uhlmann, New extension of the kalman filter to nonlinear systems, in: Signal processing, sensor fusion, and target recognition VI, Vol. 3068, Spie, 1997, pp. 182–193.

[51] E. A. Wan, R. Van Der Merwe, The unscented kalman filter for nonlinear estimation, in: Proceedings of the IEEE 2000 Adaptive Systems for Signal Processing, Communications, and Control Symposium (Cat. No. 00EX373), Ieee, 2000, pp. 153–158.

[52] Z. J. Wegert, J. Manyer, C. N. Mallon, S. Badia, V. J. Challis, Gridaptopopt.jl: a scalable julia toolbox for level set-based topology optimisation, Structural and Multidisciplinary Optimization 68 (1) (2025) 22. doi:10.1007/s00158-024-03927-3.

[53] C. G. Broyden, The convergence of a class of double-rank minimization algorithms. i. general considerations, IMA Journal of Applied Mathematics 6 (1) (1970) 76–90. doi:10.1093/imamat/6.1.76.

[54] Ordinarydiffeq.jl, https://github.com/SciML/OrdinaryDiffEq.jl, gitHub repository, accessed 2026.

[55] C. Tsitouras, Runge–kutta pairs of order 5(4) satisfying only the first column simplifying assumption, Computers & Mathematics with Applications 62 (2) (2011) 770–775. doi:https://doi.org/10.1016/j.camwa.2011.06.002.
URL https://www.sciencedirect.com/science/article/pii/S0898122111004706

[56] J. Guckenheimer, P. Holmes, Nonlinear Oscillations, Dynamical Systems, and Bifurcations of Vector Fields, Vol. 42 of Applied Mathematical Sciences, Springer-Verlag, New York, 1983. doi:10.1007/978-1-4612-1140-2.

[57] F. Martinuzzi, C. Rackauckas, A. Abdelrehim, M. D. Mahecha, K. Mora, Reservoircomputing.jl: An efficient and modular library for reservoir computing models, Journal of Open Source Software 7 (78) (2022) 4520. doi:10.21105/joss.04520.

[58] B. van der Pol, On "relaxation-oscillations", The London, Edinburgh, and Dublin Philosophical Magazine and Journal of Science 2 (11) (1926) 978–992. doi:10.1080/14786442608564127.

[59] A. N. Brooks, T. J. R. Hughes, Streamline upwind/Petrov–Halerkin formulations for convection dominated flows with particular emphasis on the incompressible navier–Stokes equations, Computer Methods in Applied Mechanics and Engineering 32 (1–3) (1982) 199–259. doi:10.1016/0045-7825(82)90071-8.

[60] F. Zacchei, P. Conti, A. Frangi, A. Manzoni, Multi-fidelity delayed acceptance: Hierarchical mcmc sampling for bayesian inverse problems combining multiple solvers through deep neural networks, Computer Methods in Applied Mechanics and Engineering 456 (2026) 118916. doi:https://doi.org/10.1016/j.cma.2026.118916.
URL https://www.sciencedirect.com/science/article/pii/S0045782526001891

APPENDIX A. APPENDIX A: MISSING CODE SNIPPET FROM THE VAN DER POL EXAMPLE

In Listing 22 we collect the code snippet omitted from the Van der Pol example for brevity.

bias_aware_oscillator.jl

```julia
using GridapROMs
using LinearAlgebra
using Opals
using OrdinaryDiffEq
using Random

# Time discretisation and parametric space
pdomain = (20.0,120.0,20.0,120.0,0.1,10.0)
pspace = ParamSpace(pdomain)
dt = 1e-4
dt_obs = 5*dt
ts = TimeStencils(;
  dt,dt_obs,t0=0.0,
  t_warmup=2.0,t_train=1.1,t_wash=2.1e-2,
  t_da=1.0
)

# Dynamical system
function oscillator!(du,u,p,t)
  ω = 240*pi
  η,ξ = u
  ζ,β,κ = p
  du[1] = ξ
  du[2] = -ω^2*η + ξ*(β-ζ) - ξ*(κ*η^2)/(1+(κ/β)*η^2)
end

# Initial condition
u0 = ParamArray([[0.1,0.1]])
```

FIGURE 22. Missing code snippet from the Van der Pol example.

APPENDIX B. APPENDIX B: MISSING CODE SNIPPET FROM THE NAVIER-STOKES EXAMPLE

Although Listing 23 appears to be quite convoluted, it follows a similar structure to Listing 22, with the only main difference being that an initial condition is manually set as the solution of a steady-state Stokes problem at $t = 0$, and several FE-specific quantities are introduced. This requires several additional lines of code to set up the workflow of this numerical experiment, but the underlying logic remains the same as in the previous examples.

navier_stokes.jl

```julia
using Gridap
using GridapGmsh
using Gridap.MultiField
using Gridap.TensorValues
using GridapSolvers.NonlinearSolvers
using GridapROMs
using GridapROMs.ParamDataStructures
using LinearAlgebra
using Opals

# Space/time discretisation and parametric space
# 1st parameter: inflow velocity magnitude
# 2nd parameter: kinematic viscosity

const umin = 0.1
const umax = 0.4
const νmin = 1e-5
const νmax = 1e-4
pdomain = (umin,umax,νmin,νmax)
pspace = ParamSpace(pdomain)

const D = 0.04
const H = 0.1795
const h₀ = D/15

const dt = 1.0*(h₀/umax)
const nt_warmup = 40
const nt_da = 80
const nt = nt_warmup + nt_da

ts = TimeStencils(;
  dt,dt_obs=2*dt,t0=0.0,
  t_warmup=nt_warmup*dt,t_da=nt_da*dt
)

tgrid = 0.0:dt:nt*dt
ptspace = TransientParamSpace(pdomain,tgrid)

# Import mesh and define FE spaces
mshdir = datadir("meshes/square.msh")
model = GmshDiscreteModel(mshdir)
Ω = Interior(model)
Γout = Boundary(model,tags="outflow")
Γin = Boundary(model,tags="inlet")
Γside = Boundary(model,tags="sides")
Γwall = Boundary(model,tags="walls")

uin(μ,t) = x -> VectorValue(μ[1],0.0)
uinμt(μ,t) = parameterise(uin,μ,t)
uwall(μ,t) = x -> VectorValue(0.0,0.0)
uwallμt(μ,t) = parameterise(uwall,μ,t)

ν(μ,t) = x -> μ[2]
νμt(μ,t) = parameterise(ν,μ,t)

order = 2
reffeᵤ = ReferenceFE(
  lagrangian,VectorValue{2,Float64},order
)
reffeₚ = ReferenceFE(lagrangian,Float64,order-1)

V = TestFESpace(
  Ω,reffeᵤ,
  dirichlet_tags=["inlet","sides","walls"],
  dirichlet_masks=[(true,true),(false,true),(true,true)]
)
Q = TestFESpace(Ω,reffeₚ)
U = TransientTrialParamFESpace(V,[uinμt,uwallμt,uwallμt])
P = TransientTrialParamFESpace(Q)
Y = MultiFieldFESpace([V,Q])
X = MultiFieldFESpace([U,P])

degree = 2*order
dΩ = Measure(Ω,degree)
dΓout = Measure(Γout,degree)
nΓout = get_normal_vector(Γout)
dΓwall = Measure(Γwall,degree)
nΓwall = get_normal_vector(Γwall)

# Stabilised weak form of the Navier-Stokes equations
Rᵤ(μ,t,u,p) = ∂t(u) + ∇(u)'⋅u + ∇(p) - νμt(μ,t)*Δ(u)
Lᵤᵃ(u,v,w) = ∇(v)'⋅u
c₁ = 12; c₂ = 4.0
Δx₀ = lazy_map(dx->dx^(1/2),get_cell_measure(Ω))
τᵤ(a) =
  1.0 / (c₁*νmin/(Δx₀.^2) + c₂*((a⋅a).^(1/2)+1e-10)/Δx₀)

res(μ,t,(u,p),(v,q)) =
  ∫( ∂t(u)⋅v + (u⋅∇(u))⋅v + 2νμt(μ,t)*(ε(u)⊙ε(v))
  - p*(∇⋅v) + (∇⋅u)*q )dΩ +
  ∫( Rᵤ(μ,t,u,p) ⋅ ((τᵤ(u))*Lᵤᵃ(u,v,q)) )dΩ

feop = TransientParamOperator(res,ptspace,X,Y)

function initial_operator()
  uin(μ) = x -> VectorValue(μ[1],0.0)
  uinμ(μ) = parameterise(uin,μ)
  uwall(μ) = x -> VectorValue(0.0,0.0)
  uwallμ(μ) = parameterise(uwall,μ)
  U₀ = ParamTrialFESpace(V,[uinμ,uwallμ,uwallμ])
  P₀ = ParamTrialFESpace(Q)
  X₀ = MultiFieldFESpace([U₀,P₀])
  u̇₀(μ) = x -> VectorValue(0.0,0.0)
  u̇₀μ(μ) = parameterise(u̇₀,μ)
  ṗ₀(μ) = x -> 0.0
  ṗ₀μ(μ) = parameterise(ṗ₀,μ)
  ẋₕ₀μ(μ) = interpolate_everywhere([u̇₀μ(μ),ṗ₀μ(μ)],X₀(μ))
  res₀(μ,(u,p),(v,q)) =
    ∫( 2νμt(μ,0.0)*(ε(u)⊙ε(v)) - p*(∇⋅v) + (∇⋅u)*q )dΩ
  ParamOperator(res₀,pspace,X₀,Y)
end

# ODE solver
nls = NewtonSolver(
  LUSolver();rtol=1e-10,maxiter=10,verbose=true
)
ode_solver = GeneralisedAlpha1(nls,dt,0.9)

# Initial condition
feop₀ = initial_operator()
ode_solver₀ = ThetaMethod(nls,dt,1.0)

function initial_condition(r)
  μ = get_params(r)
  x₀, = solve(nls,feop₀,μ)
  (r₀,xₜ₀), = solve(ode_solver₀,feop,r,x₀)
  ẋₜ₀ = get_free_dof_values(ẋₕ₀μ(μ))
  (xₜ₀,ẋₜ₀)
end
```

FIGURE 23. Missing code snippet from the Navier Stokes example.

APPENDIX C. APPENDIX C: MISSING CODE SNIPPET FROM THE HEAT EQUATION EXAMPLE

In Listing 24, we only underline that the unknown parameters are sought in the parametric domain $(1, 10)^3$, and that all transition operators are initialised from a homogeneous initial condition $u^0 = 0$ at $t = 0$.

rom_kriging_calibration.jl

```julia
using Gridap
using GridapROMs
using LinearAlgebra
using Opals

# Space/time discretisation and parametric space
pdomain = (1,10,1,10,1,10)
nt_warmup = 20
nt_da = 30
nt = nt_warmup + nt_da
dt = 0.01
t0 = 0.0
ts = TimeStencils(;
  dt,dt_obs=2*dt,t0,
  t_warmup=nt_warmup*dt,t_da=nt_da*dt
)
tgrid = t0:dt:nt*dt
ptspace = TransientParamSpace(pdomain,tgrid)

# Discrete model and FE spaces
domain = (0,1,0,1)
partition = (100,100)
model = CartesianDiscreteModel(domain,partition)
Ω = Triangulation(model)
Γn = BoundaryTriangulation(model,tags=[8])

order = 1
reffe = ReferenceFE(lagrangian,Float64,order)
V = TestFESpace(
  model,reffe;conformity=:H1,dirichlet_tags=[1,3,7]
)

g(μ,t) = x -> μ[1]*exp(-x[2]/μ[3])
gμt(μ,t) = parameterise(g,μ,t)
U = TransientTrialParamFESpace(V,gμt)

degree = 2*order
dΩ = Measure(Ω,degree)
dΓn = Measure(Γn,degree)

# Weak form of the transient heat equation
a(μ,t) = x -> 1+exp(-sin(t)^2*x[1]/sum(μ))
aμt(μ,t) = parameterise(a,μ,t)
f(μ,t) = x -> 1.
fμt(μ,t) = parameterise(f,μ,t)
h(μ,t) = x -> abs(cos(t/μ[2]))
hμt(μ,t) = parameterise(h,μ,t)

stiffness(μ,t,u,v,dΩ) = ∫(aμt(μ,t)*∇(v)⋅∇(u))dΩ
mass(μ,t,uₜ,v,dΩ) = ∫(v*uₜ)dΩ
rhs(μ,t,v,dΩ,dΓn) = ∫(fμt(μ,t)*v)dΩ + ∫(hμt(μ,t)*v)dΓn
res(μ,t,u,v,dΩ,dΓn) = mass(μ,t,∂t(u),v,dΩ) +
  stiffness(μ,t,u,v,dΩ) - rhs(μ,t,v,dΩ,dΓn)

trian_res = (Ω,Γn)
trian_jac = (Ω,)
domains = FEDomains(trian_res,(trian_jac,trian_jac))
feop = TransientLinearParamOperator(
  res,(stiffness,mass),ptspace,U,V,domains
)

# Initial condition
u0(μ) = x -> 0.0
u0μ(μ) = parameterise(u0,μ)
uh0μ(μ) = interpolate_everywhere(u0μ(μ),U(μ,t0))

# Solver
θ = 1.0
solver = ThetaMethod(LUSolver(),dt,θ)
```

FIGURE 24. Missing code snippet from the Heat equation example.